




Peptide ligands for the affinity purification of adeno-associated viruses from HEK 293 cell lysates

Wenning Chu¹  | Shriarjun Shastry^{1,2} | Eduardo Barbieri¹ | Raphael Prodromou¹ | Paul Greback-Clarke² | Will Smith² | Brandyn Moore¹ | Ryan Kilgore¹ | Christopher Cummings² | Jennifer Pancorbo² | Gary Gilleskie²  | Michael A. Daniele^{3,4} | Stefano Menegatti^{1,2,3,5} 

¹Department of Chemical and Biomolecular Engineering, North Carolina State University, Raleigh, North Carolina, USA

²Biomanufacturing Training and Education Center (BTEC), North Carolina State University, Raleigh, North Carolina, USA

³North Carolina Viral Vector Initiative in Research and Learning (NC-VVIRAL), North Carolina State University, Raleigh, North Carolina, USA

⁴Joint Department of Biomedical Engineering, North Carolina State University and University of North Carolina at Chapel Hill, Raleigh, North Carolina, USA

⁵LigaTrap Technologies LLC, Raleigh, North Carolina, USA

Correspondence

Wenning Chu.

Email: wchu3@ncsu.edu

Michael A. Daniele.

Email: mdaniel6@ncsu.edu

Stefano Menegatti.

Email: smenega@ncsu.edu

Funding information

North Carolina Viral Vector Initiative in Research and Learning (NC-VVIRAL); National Science Foundation, Grant/Award Numbers: CBET 1743404, CBET 1653590; Novo Foundation, Grant/Award Number: NNF19SA0035474; Food and Drug Administration, Grant/Award Number: R01FD007481

Abstract

Adeno-associated viruses (AAVs) are the vector of choice for delivering gene therapies that can cure inherited and acquired diseases. Clinical research on various AAV serotypes significantly increased in recent years alongside regulatory approvals of AAV-based therapies. The current AAV purification platform hinges on the capture step, for which several affinity resins are commercially available. These adsorbents rely on protein ligands—typically camelid antibodies—that provide high binding capacity and selectivity, but suffer from low biochemical stability and high cost, and impose harsh elution conditions (pH < 3) that can harm the transduction activity of recovered AAVs. Addressing these challenges, this study introduces peptide ligands that selectively capture AAVs and release them under mild conditions (pH = 6.0). The peptide sequences were identified by screening a focused library and modeled in silico against AAV serotypes 2 and 9 (AAV2 and AAV9) to select candidate ligands that target homologous sites at the interface of the VP1-VP2 and VP2-VP3 virion proteins with mild binding strength ($K_D \sim 10^{-5}$ – 10^{-6} M). Selected peptides were conjugated to Toyopearl resin and evaluated via binding studies against AAV2 and AAV9, demonstrating the ability to target both serotypes with values of dynamic binding capacity ($DBC_{10\%} > 10^{13}$ vp/mL of resin) and product yields (~50%–80%) on par with commercial adsorbents. The peptide-based adsorbents were finally utilized to purify AAV2 from a HEK 293 cell lysate, affording high recovery (50%–80%), 80- to 400-fold reduction of host cell proteins (HCPs), and high transduction activity (up to 80%) of the purified viruses.

KEYWORDS

adeno-associated virus, affinity chromatography, HEK 293 lysate, peptide ligands, virus purification

Wenning Chu and Shriarjun Shastry contributed equally to this study.

This is an open access article under the terms of the Creative Commons Attribution-NonCommercial-NoDerivs License, which permits use and distribution in any medium, provided the original work is properly cited, the use is non-commercial and no modifications or adaptations are made.

© 2023 The Authors. *Biotechnology and Bioengineering* published by Wiley Periodicals LLC.

1 | INTRODUCTION

Gene therapy provides a unique approach to cure inherited and acquired diseases by downregulating or replacing a defective gene with a functional one (Das et al., 2015; Drouin & Agbandje-McKenna, 2013). As of 2022, almost 3000 gene therapy clinical trials have been initiated (Ginn et al., 2018; Petrich et al., 2020) and four gene therapy products approved by the Food and Drug Administration (FDA) (Eisenman, 2019; Ginn et al., 2018; Petrich et al., 2020). A key role in the gene therapy revolution is played by viral vectors, owing to their ability to deliver a genomic payload efficiently and selectively to a target cell or tissue. While several classes of viral vectors are known and utilized today—employed in cell engineering (e.g., Lentivirus and Baculovirus) (Fumagalli et al., 2022; Magrin et al., 2022; Milone & O'Doherty, 2018) or vaccination and oncolytic applications (e.g., adenovirus and herpes simplex virus) (Leikas et al., 2022; Nadeau & Kamen, 2003; Wold & Toth, 2013)—the field of gene therapy is dominated by adeno-associated viruses (AAVs) (Kaplitt et al., 2007; Keeler & Flotte, 2019; Li & Samulski, 2020; Naso et al., 2017; Samulski & Muzyczka, 2014; Wang et al., 2019) owing to their low toxicity/pathogenicity and efficient integration of the transgene into the host cells.

AAV is a small, nonenveloped icosahedral virus, whose capsid can pack a linear single-strand DNA (ssDNA) genome of up to about 5 kilobases (Chamberlain et al., 2016; Lai et al., 2010; Linden et al., 1996; Vasileva & Jessberger, 2005). AAV capsids are formed by three virion proteins (VP1, VP2, and VP3), typically assembled in a 1:1:10 ratio (Nam et al., 2007). To date, 13 distinct AAV serotypes (AAV1–AAV13) are known—with the AAV2 being the most studied (Schmidt et al., 2008)—which share a 65%–99% sequence identity in their VPs and a 95%–99% structural identity (Drouin & Agbandje-McKenna, 2013; Mandel, 2004). The biomolecular variations among serotypes translate in specific cell/tissue tropism: cardiac, skeletal, and muscle cells are targeted by AAV1, AAV6, and AAV9; retina cells by AAV2 and AAV8; hepatocytes by AAV8, AAV9, and AAV-DJ; lung cells by AAV5, AAV6, and AAV9; cells in the central nervous system (CNS) by AAV1, AAV5, AAV6, AAV9, and AAV-rh10 (AAV Serotypes and AAV Tissue-Specific Tropism; Gao et al., 2004; Wang et al., 2019; Zincarelli et al., 2008). Recently, recombinant AAVs (rAAVs) have been introduced, which feature improved gene packing and tissue tropism as well as lower immunogenicity and hepatotoxicity (Muhuri et al., 2021).

The manufacturing of AAVs relies on two expression systems, namely triple transfected human embryonic kidney (HEK 293) cells, which generate $\sim 10^{14}$ vector genome-containing particles (vg) per liter of cell culture when harvested just 72 h posttransfection and are ideal for serving small cohort of patients, such as those suffering from rare diseases (Grieger et al., 2016); and the live baculovirus infection of *Spodoptera frugiperda* (Sf9) insect cells, which can be grown in serum-free media and avoid the replication of contaminating human agents, and are ideal for large AAV batches, (Rumachik et al., 2020) such as those dedicated to fighting cancer and specific monogenic diseases (Ginn et al., 2018; Hagen et al., 2014).

The large number of particles needed for a single patient dosing, which can reach up to 10^{14} vg/kg of body weight (Hinderer et al., 2018; McIntosh et al., 2013) combined with stringent requirements of purity puts significant pressure on the downstream segment of the manufacturing process. The current platform process for AAV purification—reminiscent of the one established for mAbs—begins with an affinity-based capture step, which is tasked with removing most of the host cell proteins (HCPs) and DNA (hcDNA), and concentrating the AAV product for the subsequent steps of polishing and enrichment of full capsids (Okada et al., 2009; Qu et al., 2007; Wang et al., 2019). Current affinity adsorbents include chromatographic resins functionalized with heparin (Clark et al., 1999; Summerford & Samulski, 1998) whose applicability is limited to AAV2 (Adams et al., 2020; Clément & Grieger, 2016; Wu et al., 2006) or camelid single-domain antibodies (Mietzsch et al., 2020). The latter include AVB Sepharose™ High-Performance resin, which targets AAV serotypes 1, 2, 3, and 5 (Cytiva); the POROS™ Capture-Select™ AAVX affinity resin, which targets AAV1–AAV8, AAVrh10, and rAAVs (Thermo Scientific™. POROS™ CaptureSelect™ AAV Resins: AAV8, AAV9, AAVX; Thermo Scientific™. POROS™ CaptureSelect™ AAVX Affinity Resin); POROS™ CaptureSelect AAV8 and AAV9 resins, specific to AAV8 and AAV9 (Thermo Scientific™. POROS™ Capture-Select™ AAV Resins: AAV8, AAV9, AAVX; Thermo Scientific™. POROS™ CaptureSelect™ AAV8 Affinity Resin; Thermo Scientific™. POROS™ CaptureSelect™ AAV9 Affinity Resin); and AVIPure® AAV2, AAV8, and AAV9 affinity resins (AVIPure®—AAV Affinity Resins). Despite their excellent binding capacity ($>10^{13}$ vp/mL of resin) and selectivity (Blessing et al., 2019; Smith et al., 2009) these adsorbents feature high cost, low biochemical stability, and short lifetime (<20 cycles), and require harsh elution conditions (pH < 3.0) that can cause denaturation and aggregation of the AAV capsids, with consequent loss of transduction activity of the product (Cytiva; Thermo Scientific™. POROS™ CaptureSelect™ AAV Resins: AAV8, AAV9, AAVX; Thermo Scientific™. POROS™ Capture-Select™ AAVX Affinity Resin; Thermo Scientific™. POROS™ Capture-Select™ AAV9 Affinity Resin).

In seeking robust alternatives to protein ligands, we developed an ensemble of synthetic peptides that bind AAVs selectively, enable their elution under near-physiological conditions, and can be reused multiple times without losing binding strength and selectivity. The peptide ligands presented in this work target conserved binding sites found in all AAV serotypes (i) via multisite interactions, which provide the necessary binding strength and capacity for effective product capture, although (ii) the single AAV:peptide complexes can be easily dissociated, thus enabling high product recovery at mild elution conditions.

2 | RESULTS AND DISCUSSION

2.1 | Selection of AAV-targeting ligands via rational design and screening of combinatorial peptide libraries

The biomolecular features that differentiate the various AAV serotypes—namely, the amino acid sequences of the virion proteins

VP1, VP2, and VP3, and their unique arrangement within the capsid—also determine their behavior in terms of tissue tropism, transduction efficiency, and patient safety (Asokan et al., 2010, 2012). Key domains are displayed on the protrusions found on the fivefold cylinder and on the lines drawn between two contiguous threefold axes, and the two- and fivefold axes (Drouin & Agbandje-McKenna, 2013). As active sites, however, these domains are not suitable binding targets, since the association and dissociation with affinity ligands may cause structural and biochemical alterations leading to unwanted loss of tissue tropisms and transduction efficiency. Conversely, highly conserved regions (CRs) are found in all serotypes' capsids, including a core eight-stranded β -barrel motif ($\beta\text{B}-\beta\text{I}$) and an α -helix (αA) (DiMattia et al., 2012; Drouin & Agbandje-McKenna, 2013; Xie et al., 2002) on the convex side of the VPs (Supporting Information: Figure S1A), that are not implicated in receptor binding, transduction, and antigenic specificity. These represent ideal target regions to universal AAV-binding peptides serving as ligands for serotype-independent purification of AAVs from recombinant fluids. To gather molecular-level insight in the molecular landscape of the AAV surface, we performed an *in silico* “druggability” study of the CRs using PockDrug (Borrel et al., 2015; Hussein et al., 2015) and identified five candidate sites whose morphology and physicochemical properties are suitable for docking peptide ligands (Supporting Information: Figure S1B,C and Table S1).

The physicochemical properties of the selected sites guided the design of a peptide library for the selection of candidate ligands: (i) a chain length of six or eight monomers was chosen based on the average size of the pockets (Van der Waals volume $\sim 950\text{--}1150 \text{ \AA}^3$; projection area $\sim 150\text{--}250 \text{ \AA}^2$), which provides an ideal balance—based on prior knowledge (Chu et al., 2022; Lavoie et al., 2021; Prodromou et al., 2021; Reese et al., 2020; Xiao et al., 2022)—between the expected biorecognition activity and manufacturing cost; (ii) the combinatorial positions in the library were randomized with alanine, asparagine, glutamic acid, histidine, isoleucine, lysine, phenylalanine, serine, and tryptophan, which were adopted as the amino acids capable of forming a network of diverse noncovalent interactions with the selected binding pockets; and (iii) a Gly-Ser-Gly (GSG) tripeptide spacer was utilized to link the combinatorial segment of the library to the resin to improve peptide display, thus promoting the outcome of library screening and subsequent Edman sequencing. The peptide libraries were synthesized following the “split-couple-and-recombine” technique (Aina et al., 2007; Lebl et al., 1994) on ChemMatrix beads—porous, hydrophilic, translucent particles that have proven an excellent substrate for the synthesis and selection of peptide ligands (Day et al., 2019; Kish et al., 2017; Lavoie et al., 2019).

The library was incubated with a model feedstock containing red-fluorescently labeled AAV2 and green-labeled HEK 293 HCPs, and screened using a bead sorting device developed by our team for the rapid selection of peptide ligands (Day et al., 2019; Saberi-Bosari et al., 2019): AAV2 was utilized as a model target for being the most studied and utilized of the currently known human and nonhuman primate AAV serotypes (Schmidt et al., 2008); the formulation of the

feedstock—namely AAV2 at 5×10^{11} vp/mL and HEK 293 HCPs at 0.5 mg/mL—mimics industrial cell culture lysates and was adopted to identify peptide ligands capable of isolating AAV from complex sources in *bind-and-elute* mode. The device comprises a microfluidic chamber, where each bead is imaged using a multiple-wavelength fluorescence microscope, and is controlled by software performing real-time monitoring, image processing, and selection of the beads (Figure 1) (Chu et al., 2022; Kilgore et al., 2023; Prodromou et al., 2023; Sripada et al., 2022). Beads with high binding strength (i.e., ratio of the bead's vs. standard red fluorescence intensity >0.9) and selectivity (i.e., red vs. green intensity ratio >100) are retained in the device, while all other beads are discarded. Each retained bead is exposed to a flow of elution buffer, namely 1 M MgCl_2 in 20 mM Bis-Tris buffer at pH 6.0, whose composition and pH was adopted to ensure the selection of peptide ligands that enable efficient AAV release under gentle conditions (*note*: the adoption of MgCl_2 to formulate the elution buffer was inspired by prior work on the purification of alpha-1 antitrypsin; [Chu et al., 2022] where it afforded high product yield and activity; furthermore, recent studies indicated that magnesium safeguards the transduction activity of AAVs [Rambhai et al., 2020] which can be impacted rather significantly by low pH). Accordingly, only the beads displaying effective AAV elution (i.e., ratio of bead's pre- vs. postelution red fluorescence intensity >10) were selected and analyzed via Edman degradation to sequence the peptide carried thereon. The resulting 6- and 8-mer sequences are listed in Supporting Information: Table S2, while the homology analysis is in Figure 1.

2.2 | Evaluation of AAV binding and release by peptide-functionalized chromatographic resins in noncompetitive mode

Selected sequences IWWHIAKF, FWNWHHFK, FWWAAFFK, IAFK-KISI, IKIFFFFS, GYISRHPG, KFNHWF, WKAHNN, KWWIWA, WWI-KIS, FFNFFK, and FNHFFI were conjugated to Toyopearl AF-Amino-650M resin and evaluated for AAV binding and elution in noncompetitive mode to draw an initial ranking of the candidate ligands; commercial affinity adsorbents POROS™ CaptureSelect™ AAVX and AVB Sepharose HP resin were utilized as reference standards. Since different serotypes display specific tissue tropisms, (Gao et al., 2005; Wang et al., 2019) evaluating the ability of an affinity resin to target different serotypes is the first step in demonstrating its potential in downstream bioprocessing of AAVs. In this context, we adopted AAV2 and AAV9 as model serotypes: AAV2 is the most widely studied serotype to date and is the one for which the majority of values of the binding capacity of affinity adsorbents are reported in the technical literature (Kaludov et al., 2002; Merten et al., 2005; Zolotukhin et al., 2002); AAV9 has received significant attention—clinically, for its ability to bypass the blood-brain barrier (BBB) and, in the context of biomanufacturing, for being a secreted vector whose purification is challenging (*note*: affinity resins marketed as universal AAV binders often struggle

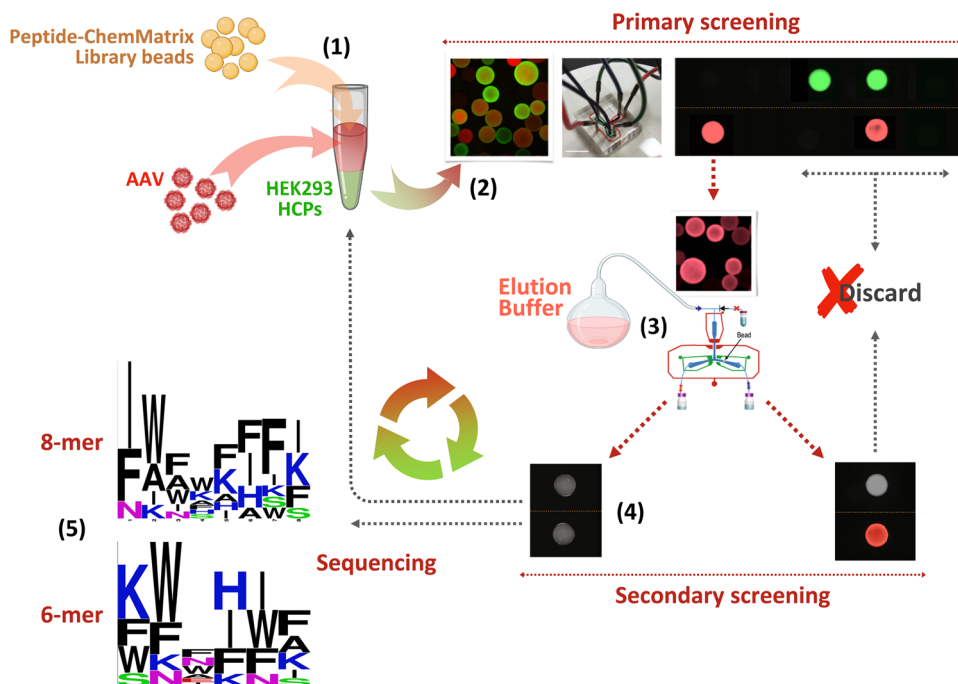


FIGURE 1 Process for identification of AAV-targeting peptide ligands. An ensemble of 6-mer or 8-mer peptide-ChemMatrix beads are (1) collectively incubated with a screening mix comprising AF594-labeled AAV2 (red) at 5×10^{11} vp/mL and AF488-labeled HEK 293 HCPs (green) at ~ 0.5 mg/mL; (2) the beads are fed to a microfluidic bead sorting device, which discards all nonfluorescent, the green-only, and red-and-green beads, and retains every red-only bead; (3) the latter is exposed to an elution buffer comprising 1 M MgCl_2 in 20 mM Bis-Tris buffer at pH 6.0 for 2 min at room temperature; (4) every bead that displays at least a 10-fold loss of red fluorescence is selected as a positive lead; (5) finally, positive beads are analyzed by Edman degradation to identify the candidate AAV-targeting peptides. Sequence homology of the selected 6-mer and 8-mer peptides prepared using Weblogo. AAV, adeno-associated viruses; HCP, host cell protein.

to capture AAV9, and dedicated adsorbents for AAV9 purification have been developed [Wang et al., 2019; Cytiva; Samaranch et al., 2012; Thermo Scientific™. POROS™ CaptureSelect™ AAVX Affinity Resin). To evaluate the peptide-based resins under industrially relevant conditions, pure AAV2 and pure AAV9 at $\sim 5 \times 10^{11}$ vp/mL in 10 mM Bis-Tris buffer at pH 7.0 were utilized as feedstocks, and loaded at a ratio of $\sim 10^{13}$ vp/mL of resin, which is expected to be the average binding capacity of the resins.

The bound AAV vectors were recovered from the peptide-Toyopearl resins under the same mild elution conditions adopted in library screening—namely, 1 M MgCl_2 in 10 mM Bis-Tris buffer at pH 6.0—while strong acidic elution (i.e., 200 mM MgCl_2 in 200 mM citrate buffer at pH 2.2 and phosphate-buffered saline (PBS) at pH 2.0, respectively, as recommended by the manufacturers) were implemented for the AAVX and AVB resins to ensure a rigorous performance evaluation of the selected ligands. The chromatograms obtained with pure AAV2 and AAV9 and the electrophoretic analysis of the collected fractions are respectively reported in Supporting Information: Figures S2 and S3, while the values of yield are reported in Figure 2.

As shown in Figure 2, all peptide resins bound AAV2 efficiently (<1.7% loss). These results corroborate the library design criteria inspired by the druggability study of AAV capsid proteins and are in line with the in-silico evaluation of AAV: peptide binding reported below. Specifically, the values of AAV2 yield provided by

KFNHWFG (45%), WKAHNKG (79.8%), IWWHIAKFG (54.9%), and FWAAFFKG (44.8%) were comparable to those granted by AAVX POROS™ (63.4%) and AVB Sepharose (45.8%) resins. Similar values of yield were obtained with AAV9: notably, IWWHIAKFG (61.7%), FWNWHHFKG (43.9%), FWAAFFKG (53.7%), KWWIWAG (57.2%), and FFNFFKG (72.4%) significantly outperformed AAVX POROS™ (25.6%) and AVB Sepharose (10.6%) resins. Notably, while the values of yield of both serotypes were comparable across the various resins, the values of product loss in the flow-through and wash were substantially higher for AAV9 than AAV2. On the other hand, the values of yield and binding strength calculated in silico ($K_{D, \text{in silico}}$, see Table 1) indicate that product loss is not due to lack of affinity by the peptides for AAV9. The electrophoretic analyses of eluted AAV2 (Supporting Information: Figure S2C) and AAV9 (Supporting Information: Figure S3D) show the presence of the capsid proteins VP1 (~ 87 kDa), VP2 (~ 73 kDa), and VP3 (~ 62 kDa) in the correct $\sim 1:1:10$ ratio (DiMattia et al., 2012; Drouin & Agbandje-McKenna, 2013; Levy et al., 2009) based on the densitometric analysis of the gels, corroborating our interpretative hypothesis that only fully formed capsids are captured by the peptide ligands (note: Supporting Information: Figure S3C shows the presence of VP2 and VP3 proteins, but not VP1, in the unbound (UB) fractions, suggesting the presence AAV9-like contaminants in the feedstock (e.g., monomeric or aggregated VP3); while not captured by the peptide-functionalized resins,

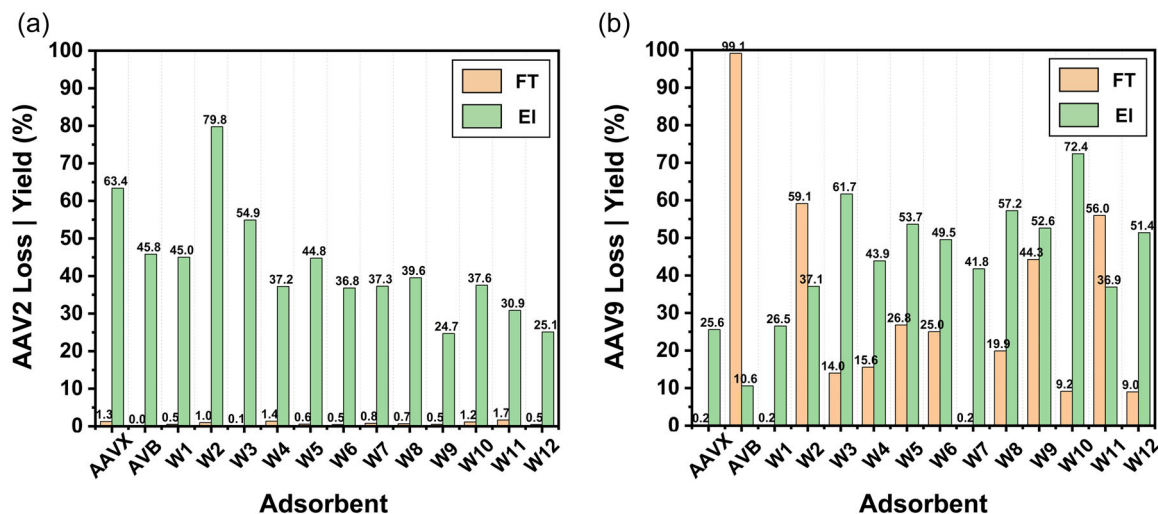


FIGURE 2 Values of loss (orange, calculated as the ratio of the AAV titer in the flow-through and wash fractions vs. load) and yield (green, calculated as the ratio of the AAV titer in the elution fraction vs. load) of (a) AAV2 and (b) AAV9 obtained via bind-and-elute studies in noncompetitive mode using peptide-based resins KFNHWFG- (W1), WKAHNKG- (W2), IWWHIAKFG- (W3), FWNWHHFKG- (W4), FWWAAFFKG- (W5), IAFKKISIG- (W6), IKIFFFSFG- (W7), KWWIWAG- (W8), WWIKISG- (W9), FFNFFKG- (W10), FNHFFIG- (W11), GYISRHPG- (W12) Toyopearl resins, and control adsorbents POROS™ CaptureSelect™ AAVX and AVB Sepharose HP resins. The AAV titer in the flow-through, wash, and elution fractions was measured using serotype-specific ELISA kits. AAV, adeno-associated viruses; ELISA, enzyme-linked immunosorbent assay; HCP, host cell protein.

TABLE 1 Values of dissociation constant ($K_{D,in\ silico}$) of the complexes formed by peptides KFNHWFG, FFNFFKG, FNHFFIG, IWWHIAKFG, FWNWHHFKG, and FWWAAFFKG with the capsids of AAV2, AAV6, AAV8, and AAV9 obtained via molecular docking and dynamics simulations.

Sequence	AAV2:peptide $K_{D,in\ silico}$ (M)		AAV6:peptide $K_{D,in\ silico}$ (M)		AAV8:peptide $K_{D,in\ silico}$ (M)		AAV9:peptide $K_{D,in\ silico}$ (M)	
	pH 6.0	pH 7.4	pH 6.0	pH 7.4	pH 6.0	pH 7.4	pH 6.0	pH 7.4
KFNHWFG	1.2×10^{-4}	1.3×10^{-6}	7.5×10^{-4}	2.0×10^{-6}	1.9×10^{-4}	2.6×10^{-6}	6.1×10^{-5}	4.6×10^{-7}
FFNFFKG	5.4×10^{-4}	1.1×10^{-6}	7.2×10^{-4}	3.7×10^{-6}	7.2×10^{-4}	1.0×10^{-5}	1.0×10^{-3}	1.3×10^{-6}
FNHFFIG	1.6×10^{-4}	9.3×10^{-7}	4.2×10^{-4}	5.2×10^{-6}	6.6×10^{-6}	1.3×10^{-7}	2.4×10^{-3}	3.7×10^{-5}
IWWHIAKFG	5.1×10^{-3}	2.4×10^{-6}	1.1×10^{-3}	2.7×10^{-6}	7.2×10^{-4}	2.9×10^{-6}	4.8×10^{-3}	1.1×10^{-5}
FWNWHHFKG	5.4×10^{-4}	1.9×10^{-6}	7.2×10^{-4}	2.4×10^{-6}	2.7×10^{-4}	5.1×10^{-5}	3.7×10^{-3}	1.3×10^{-5}
FWWAAFFKG	1.3×10^{-3}	1.7×10^{-6}	6.4×10^{-4}	2.3×10^{-6}	1.7×10^{-4}	8.1×10^{-6}	5.0×10^{-3}	2.5×10^{-5}

Note: The values of $K_{D,in\ silico}$ were derived from the average of the ΔG_b of the various VP:peptide complexes weighted by the frequency of the interfaces, namely 3.4% for VP1–VP2, 6.9% for VP1–VP3 and VP2–VP3, and 82.8% for VP3–VP3.

these impurities can be detected by enzyme-linked immunosorbent assay (ELISA), causing overestimated values of product loss in Figure 2).

Overall, the performance of the peptide ligands is rather remarkable –with respect to their protein counterparts–when one considers the difference in elution conditions (pH 6 vs. pH 2). At low pH, in fact, AAVs can undergo conformational alterations that cause capsid aggregation or loss of integrity (Drouin & Agbandje-McKenna, 2013; Nam et al., 2011); externalization of the VP1 phospholipase A2 (PLA₂) domain, which triggers capsid uncoating and release of the genetic payload (Drouin & Agbandje-McKenna, 2013; Pénczes et al., 2020; Tu et al., 2015); and biochemical alterations (e.g., hydrolysis, deamidation, or oxidation of the VPs) that impair capsid docking to the cellular receptor (AAVR), and thus

host entry and trafficking (Giles et al., 2018; Lins-Austin et al., 2020; Penzes et al., 2021). The current approach to minimizing these instances relies on immediate pH neutralization of the elution stream from POROS™ AAVX and AVB Sepharose resins. Conversely, the unique approach enabled by the peptide presented in this study aims to preserve the transduction activity of the AAV products by achieving efficient elution under near-physiological conditions.

2.3 | In silico investigation of AAV:peptide binding

The results presented above suggest that the identified peptide sequences are capable of binding not only the AAV2 capsids

employed in the library screening, but also AAV9 (Mietzsch et al., 2021). Notably, these two serotypes belong to different antigenic clades, respectively B and F, and feature rather different sequences (VP1/VP3 amino acid identity ~81%) and structures (structural identity ~94%) (Mietzsch et al., 2021; Stagg et al., 2022).

To evaluate the ability of the selected peptides to bind multiple AAV serotypes, we modeled the binding of three 6-mer (KFNHWFG, FFNFFKG, and FNHFFIG) and three 8-mer (IWWHIAKFG, FWNWHHFKG, and FWWAFFKG) peptides to the crystal structures of AAV2, AAV6, AAV8, and AAV9 capsids via molecular docking and molecular dynamics (MD). The secondary structure of the peptides, obtained via MD simulations in explicit water, were docked against a spherical cap representing the AAV capsids in HADDOCK v. 2.4 (Honorato et al., 2021; van Zundert et al., 2016). The homology spherical cap structures were obtained by collating published structures, namely PDB IDs 6U0V, 6IH9, 5IPI, and 6IHB for AAV2; 3SHM, 5EGC, 4V86, 3OAH for AAV6; 6V10, 2QA0, 3RAA, 6U2V, 6PWA for AAV8; and 3UX1, 7MT0, 7WJW, and 7WJX for AAV9. An initial round of “blind” docking was performed to evaluate—in an unbiased fashion—the ability of the selected sequences to target the homologous binding sites identified in the initial

“druggability” study (Supporting Information: Figure S1B). Additionally, to mimic the orientational constraint imposed upon the peptides by their conjugation onto the surface of the chromatographic resin, we imposed the -GSG tripeptide appended on the C-terminal end of the peptides not to bind AAV (Barozzi et al., 2020; Day et al., 2019, 2020; Mukherjee et al., 2023).

The resulting AAV:peptide complexes were refined via MD simulations (150 ns) in explicit solvent to obtain values of Gibbs free energy of binding (ΔG_b), which were used to identify putative binding sites ($|\Delta G_b| > 6.5$ kcal/mol). Notably, all binding poses identified on AAV2 and AAV9 coincided with the binding sites identified in the “druggability” study. Accordingly, a second round of peptide docking was performed on these sites upon conditioning the homology structures of the capsids to both pH 7.4 and 6.0, and the docked structures were refined via extended MD simulations (500 ns) to obtain accurate values of binding energy. Representative complexes formed by the selected peptides with AAV2, AAV6, AAV8, and AAV9 capsids at pH 7.4 are shown in Figure 3, while the values of ΔG_b and the corresponding values of dissociation constant ($K_{D,in\ silico}$) at pH 7.4 and pH 6 are listed in Table 1; finally, detailed results of peptide docking for AAV2 and AAV9 are reported in Supporting Information: Figures S4–S9.

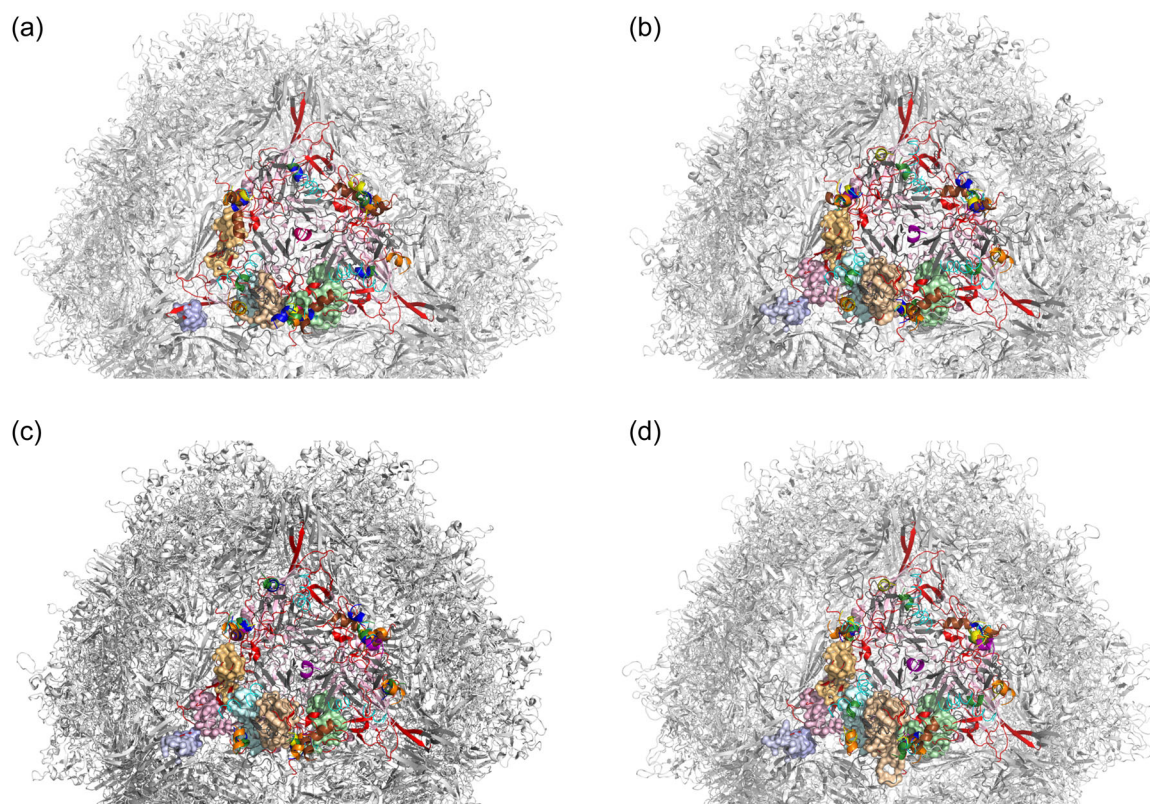


FIGURE 3 Representative complexes formed by peptides KFNHWFG (green), FFNFFKG (yellow), FNHFFIG (pink), IWWHIAKFG (brown), FWNWHHFKG (cyan), and FWWAFFKG (orange) with the capsids of (a) AAV2 (PDB IDs 5IPI, 6IH9, 6IHB, and 6U0V); (b) AAV6 (3SHM, 3OAH, 4V86, and 5EGC); (c) AAV8 (2QA0, 3RAA, 6PWA, 6U2V, and 6V10); and (d) AAV9 (3UX1, 7MT0, 7WJW, and 7WJX) obtained via molecular docking and dynamics simulations. The segments of the VP that are not solvent accessible or whose homology among AAV serotypes is lower than 95% are in gray, the homologous segments of VP that are solvent accessible and displayed on the concave side of the capsid are in pink, and the homologous segments of VP that are solvent accessible and displayed on the convex side of the capsid are in red; the binding sites are labeled in Supporting Information: Figure S1.

TABLE 2 Values of dynamic AAV2 binding capacity ($DBC_{10\%}$) of peptide-functionalized resins loaded with a feedstock containing AAV2 in the HEK 293 lysate at the titer of 3.2×10^{11} vp/mL in phosphate-buffered saline (PBS) pH 7.4 at residence time (RT) of 3 min.

Resin	$DBC_{10\%}$ (vp AAV/mL of resin)
KFNHWF-Toyopearl	1.33×10^{13}
IWWHIAKF-Toyopearl	9.53×10^{12}
FWNWHHFK-Toyopearl	8.75×10^{12}
IKIFFFFS-Toyopearl	1.02×10^{13}
FFNFFK-Toyopearl	1.40×10^{13}
POROS™ AAVX	4.60×10^{14}
AVB Sepharose	3.21×10^{14}

Confirming the criteria of library design and the results of dynamic binding in Figure 2, the *in silico* results portray the selected peptides as serotype-agnostic ligands. Specifically, the peptides consistently CRs located at the interface among different VPs, which is critical in order for AAV-binding ligands to target not only multiple serotypes but also capsids of the same serotype, given the stochastic arrangement of the VPs within a capsid. Among the docked peptides, KFNHWFG and IWWHIAKFG in particular targeted homologous binding sites located at the VP1-VP2, VP1-VP3, VP2-VP3, and VP3-VP3 interfaces, while FWNWHHFKG and FNHFFIG only targeted the VP1-VP3, VP2-VP3, and VP3-VP3 interfaces. Analogous behavior is found among anti-AAV antibodies, especially those utilized in analytical and diagnostic kits (Moskalenko et al., 2000). As portrayed in Figure 3, and in more detail in Supporting Information: Figures S4–S9, the pose of each peptide on homologous target sites located at different interfaces varies slightly due to subtle variations in the mutual orientation of the interlocking VPs. Because this translates in minor differences in the peptide:capsid binding energy, the values of $K_{D,in\ silico}$ reported in Table 2 were calculated by averaging the ΔG_b of the various poses weighted by the frequency of the interfaces (*note*: as such, the reported values of $K_{D,in\ silico}$ represent mere estimates of the peptide:VP affinity). Furthermore, peptides FNHFFIG, KFNHWFG, and IWWHIAKFG were also found to target conserved druggable domains displayed on VP3, and hence on VP1 and VP2, although they did not overlap with the binding sites of the AAV receptor (AAVR, in cyan in Supporting Information: Figures S4–S9).

Notably, the binding strength of the various site:peptide complexes was found to be rather weak compared to the values of the AAV:antibody counterparts ($K_{D,in\ silico} \sim 10^{-9}$ M). Notably, the 6-mer sequences KFNHWFG, FFNFFKG, and FNHFFIG consistently display a higher affinity, with values of $K_{D,in\ silico}$ across the four serotypes fluctuating between 10^{-6} and 10^{-7} M, whereas 8-mers IWWHIAKFG, FWNWHHFKG, and FWWAAFFKG ranked as weaker binders, with $K_{D,in\ silico} \sim 10^{-5}$ – 10^{-6} M. The trajectories of the MD simulations indeed showed that the 6-mer peptides outperformed

8-mer peptides in accessing the druggable pockets located in the valleys located between the capsid's three- and two-fold axes. Furthermore, the analysis of pairwise interactions between the residues displayed by the peptide ligands and key amino acids in the target sites of VP3 (Supporting Information: Figure S10) demonstrate the formation of a dense network of side chain-side chain and side chain-backbone hydrogen bonds as well as π - π interactions; these account, respectively, for 56%–68% and 11%–16% of the VP:peptide binding energy; notably, fewer-than-expected coulombic and hydrophobic interactions were recorded, which provided lesser contributions, respectively 8%–14% and 7%–12%, to the binding energy.

Moderate binding strength is welcome in the context of affinity chromatography of labile therapeutics. For AAV purification in particular, weak VP:peptide interactions are conducive to easier elution and reduce the risk of capsid adsorption resulting in the denaturation of the protrusions that determine tissue tropism and gene transduction to the target cells. At the same time, the peptide density on the surface of the resin is sufficient to achieve multisite interactions that grant high binding capacity and efficient product capture despite the low titer of capsids in the feedstock. Based on the values of peptide density on the resin (~ 0.12 – 0.15 mmol/g) and the resin's specific surface (~ 30 m²/g), and the projection area of each asymmetric unit on the icosahedral capsid (~ 81 nm²) (Drouin & Agbandje-McKenna, 2013) approximately 30 peptides are displayed on the area of the resin that is impacted by a single capsid. Comparing this number with the arrangement of the peptide binding poses on the triangular unit shown in Figure 3 shows the likelihood of forming 3–5 VP:peptide interactions per bound capsid. This ultimately suggests that AAV capture by the peptide-functionalized resin is governed by a multisite binding mechanism, where the μ M-level affinity of single peptides are synergized into pM/nM-level avidity, on par with AAV:antibody binding. To evaluate this effect, we conducted an isotherm adsorption study of AAV2 onto KFNHWF-Toyopearl resin. The adsorption curve in Supporting Information: Figure S11 shows a maximum capacity Q_{max} of 3.8×10^{13} vp/mL of resin and a $K_{D,isortherm} \sim 9 \times 10^{10}$ vp/mL (corresponding to 0.16 pM). The value of equilibrium binding capacity is in line with the values measured in dynamic conditions (Table 2), while the remarkably low value of $K_{D,isortherm}$ corroborates the claim of avidity-driven AAV adsorption onto the peptide-functionalized resin. At the same time, we also speculate that potential heterogeneities in the display of peptides on the resin surface and the variability in the pose by which the capsid adsorbs onto the peptide-functionalized substrate may reduce the strength of capture, thus preventing irreversible adsorption of the loaded capsids; where ideal binding occurs, however, the mild elution conditions may fail to recover the adsorbed capsids, which are released later during regeneration.

Following the description of the adsorption step, the *in silico* results also help elucidate AAV elution under mild conditions by offering a mechanism of capsid dissociation from the resin-bound peptides. Specifically, the MD simulations show that the residues located at the periphery and in the immediate surrounding of the

binding sites participate in a cyclical opening/closing conformational change. Decreasing the pH from 7.4 to 6.0 lowers the electrostatic charge of the binding sites by neutralizing the histidine residues ($pK_a \sim 6.0$), the majority of which are neighbored by other cationic (i.e., lysine and arginine) or anionic (i.e., aspartate and glutamate); the analysis of primary sequences reported on PDB for AAV2 (6U0V), AAV6 (3SHM), AAV8 (6V10), and AAV9 (3UX1), indicates that 64% of histidine residues are either neighbored by a charged residue either immediately or with one interposing amino acid. As the local network of electrostatic bonds decrease upon acidification, the conformational flexibility of the binding sites increases, and so does the pulsatile behavior of the binding sites. As observed in prior work (Mukherjee et al., 2023) oscillation and distortion of the pairwise interactions result in lower VP:peptide binding strength: specifically, the values of $|\Delta G_b|$ averaged over the last 100 ns of MD simulations decrease between pH 7.4 and 6.0 of ~ 3.5 kcal/mol for AAV2, ~ 3.3 kcal/mol for AAV6, ~ 2.2 kcal/mol for AAV8, and ~ 3.2 kcal/mol for AAV9. This ultimately translates in 50- to 200-fold variations in binding strength ($K_{D, \text{in silico}}$), which is consistent with the high values of recovery obtained experimentally. Furthermore, the addition of Mg^{2+} —a kosmotropic cation—in the elution buffer promotes a salting-in effect, leading to the hydration of the binding sites and their dissociation from the ligands. This combination of conformational pulsing and salting-in of the binding sites represents a powerful elution trigger and supports the high values of AAV yield granted by the peptide ligands.

Collectively, the *in silico* results corroborate the experimental observations that the selected sequences bind AAVs in a serotype-agnostic manner and afford efficient elution of bound capsids under mild conditions.

2.4 | Purification of AAV from HEK 293 cell culture lysate using peptide-functionalized chromatographic resins

Having confirmed the broad targeting activity, high binding capacity, and efficient elution under mild conditions of the peptide ligands, we moved to evaluate their ability to purify AAV2 from a clarified HEK 293 cell culture lysate. The feedstock was formulated to mimic the harvests typical of the gene therapy industry (AAV2 titer $\sim 1.6 \times 10^{11}$ vp/mL; HCP titer ~ 0.5 mg/mL). A relatively short RT ~ 3 min was adopted for the binding step to capitalize on the high AAV binding capacity of the peptide-based adsorbents while attempting to minimize the adsorption of HEK 293 HCPs. The chromatograms of AAV2 purification are collated in Supporting Information: Figure S12, while the size exclusion chromatography (SEC) and steric exclusion chromatography (SEC) analyses of the collected fractions are reported in Supporting Information: Figures S13 and S14, respectively; finally, the values of AAV2 yield and logarithmic removal values of HEK 293 host cell proteins (HCP LRV) are summarized in Figure 4.

The results in Figure 4 mirror the values of AAV2 capture and release presented in Figure 2a: (i) product loss in the flow-through and wash fractions oscillated between 1% and 4%, indicating that the adsorbents maintain their high binding capacity when loaded with complex feedstocks; (ii) the peptide-based adsorbents afforded yields ranging between 40% and 65%, thus consistently outperforming reference POROS™ CaptureSelect™ AAVX Affinity and AVB Sepharose HP resins; and (iii) 6 out of 12 peptide-based adsorbents afforded values of HCP LRV above 1.8, with IWWHIAKFG-Toyopearl and FWNWHHFKG-Toyopearl resins achieving LRVs of 2.6 and 2.5,

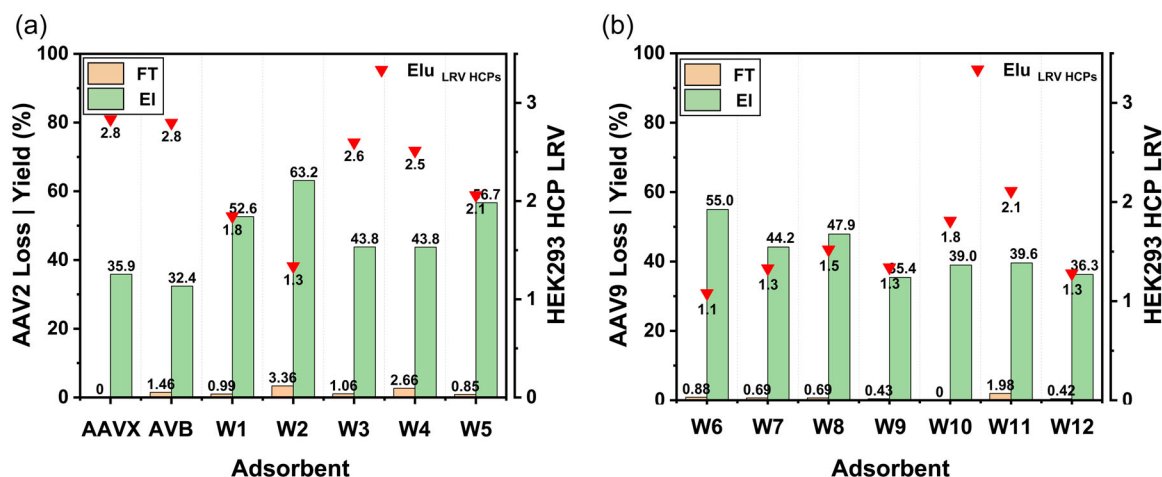


FIGURE 4 Values of loss (orange, calculated as the ratio of the AAV titer in the flow-through and wash fractions vs. load) and yield (green, calculated as the ratio of the AAV titer in the elution fraction vs. load) of AAV2 and logarithmic reduction of HCPs (HCP LRV, red triangles) obtained via chromatographic purification of AAV2 from a clarified HEK 293 cell lysate (AAV2 titer: $\sim 1.6 \times 10^{11}$ vp/mL; HCP titer: ~ 0.5 mg/mL) using (a) control adsorbents POROS™ CaptureSelect™ AAVX and AVB Sepharose HP resins as well as peptide-based resins KFNHWFG- (W1), WKAHNKG- (W2), IWWHIAKFG- (W3), FWNWHHFKG- (W4), FWWAAFFKG- (W5), (b) IAFKKISIG- (W6), IKIFFFSG- (W7), KWWIWAG- (W8), WWIKISG- (W9), FFNFFKG- (W10), FNHFFIG- (W11), GYISRHPG- (W12) Toyopearl resins. The AAV titer in the flow-through, wash, and elution fractions was measured using serotype-specific ELISA kits. AAV, adeno-associated viruses; ELISA, enzyme-linked immunosorbent assay; HCP, host cell protein.

respectively—corresponding to a 400- and 330-fold reduction of HEK 293 HCPs—thus providing a purification performance comparable to that of commercial reference resins.

The feedstock and elution fractions were further analyzed via SEC (Supporting Information: Figure S13) and SXC (Supporting Information: Figure S14) to evaluate the presence of capsid aggregates and fragments, and visualize the removal of process-related impurities (*note*: while HEK 293 ELISA assays provide the titer of HCPs, analytical chromatography also reveals the presence of denatured or hydrolyzed HCPs, other nonproteinaceous metabolites, host cell DNA and RNA, and media components); and transduction assay on human epithelial cells (HT1080) to evaluate the recovery of the genetic payload and the infectivity of the purified viruses, respectively.

The SEC and SXC analyses exemplify the complex biomolecular landscape of the feedstock (Supporting Information: Figures S13A and S14A). Mirroring the ELISA results, the chromatographic profiles of the fractions eluted from POROS™ CaptureSelect™ AAVX Affinity (Supporting Information: Figures S13B and S14B) and AVB Sepharose HP (Supporting Information: Figures S13C and S14C) resins highlight the high purity of the eluted AAV2; notably, despite the harsh elution pH, no aggregates were observed in those fractions, potentially owing to the salting-in effect provided by the salt composition and concentration of the respective elution buffers. The viruses eluted from the peptide-based adsorbents are accompanied by some impurities, although the chromatographic profiles of the eluted fractions from IWWHIAKFG- (~205-fold reduction of impurities based on the chromatographic area), FWNWHHFKG- (~160-fold), FWAAFFKG- (185-fold), FFNFFKG- (135-fold), and FNHFFIG-Toyopearl (145-fold) resins—in line with the results of the ELISA kits—demonstrate the excellent purification activity of the selected peptide ligands.

Together with yield and purity, the transduction activity of the eluted viral vectors—namely, their ability to effectively deliver their gene payload to the target cells—is a critical parameter that defines the quality of the purification process. Unlike antibody-based therapeutics, whose biomolecular stability allows leveraging significant variations in buffer conductivity and pH to control their adsorption to and elution from the affinity resins, AAVs are significantly more susceptible to loss of activity driven by bioprocess conditions. Commercial affinity resins for AAV purification, however, mandate product elution under extremely acidic pH, varying between two and three depending upon serotype and desired elution yield (>50%) and titer. Conversely, the peptide-based adsorbents presented in this work afford comparable elution performance under significantly milder conditions (1 M MgCl₂ in the 20 mM Bis-Tris buffer at pH 6.0). Accordingly, we resolved to quantify the transduction activity of the AAV2 purified using the peptide-based adsorbents versus the reference AVB Sepharose HP, and Capture-Select™ AAVX Affinity resins on human epithelial (HT1080) cells. The transgene encapsidated in the model AAV2 utilized in this study encodes for green fluorescence protein (GFP), thus allowing facile quantification of transduction activity via fluorescence flow

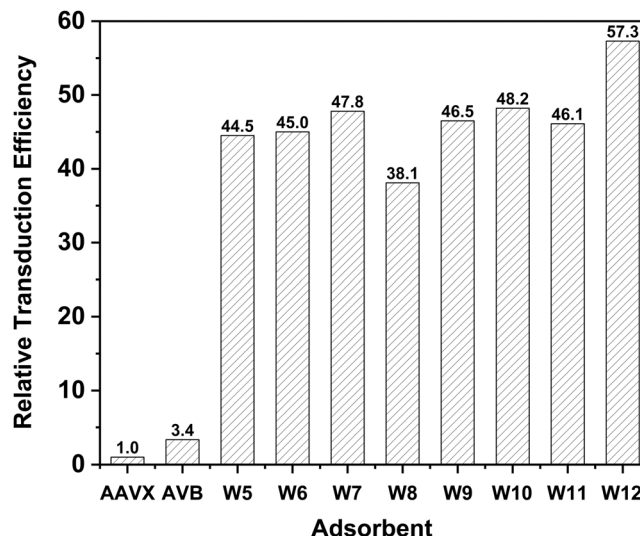


FIGURE 5 Values of relative transduction efficiency of AAV2 purified from a clarified HEK 293 cell lysate using peptide-based adsorbents FWAAFFKG-, IAFKKISIG-, IKIFFFSFG-, KWWIWAG-, WWIKISG-, FFNFFKG-, FNHFFIG-, and GYISRHPG-Toyopearl resins. The transduction efficiency (TU/vp) of eluted AAV2 was measured on human epithelial (HT1080) by performing a green fluorescence assay using a CytoFLEX Flow Cytometer. The values of relative transduction efficiency were calculated as the ratio of transduction efficiency of the AAV2 eluted from a peptide-based adsorbent versus the transduction efficiency of the AAV2 eluted from POROS™ CaptureSelect™ AAVX Affinity resin.

cytometry (FFC). The results collated in Figure 5 corroborate the claim that elution under mild conditions affords a product with superior transduction activity: the AAV2 purified using peptide-based adsorbents transduced in fact a remarkably higher amount of HT1080 cells, up to 20- to 60-fold more than the AAV2 eluted from commercial affinity resins. This outcome can also be attributed to the ability of the peptide-functionalized resins to preferentially capture gene-loaded capsids: the quantification of viral genomes in the eluted fractions via quantitative polymerase chain reaction (qPCR) indicated in fact that IAFKKISIG-, IKIFFFSFG-, FFNFFKG-, and GYISRHPG-Toyopearl resins enriched the full capsid titer from <5% in the feedstock to 6.4%, 12.4%, 14.7%, and 7.4%, respectively.

To evaluate the reusability of the peptide-functionalized resins, IKIFFFS-Toyopearl resin was utilized for five successive cycles of AAV2 purification, each followed by a cleaning step with aqueous 0.5 M NaOH. The results reported in Supporting Information: Figure S15 indicate that the resin maintained its purification activity despite the harsh cleaning conditions (*note*: the recommended cleaning-in-place protocol for POROS™ CaptureSelect™ AAVX and AVB Sepharose affinity resins is with 10–25 mM NaOH).

Having compared the purification performance of the various peptides, we resolved to conclude this study by measuring the dynamic binding capacity (DBC_{10%}) of selected adsorbents KFNHWFG-, IWWHIAKFG-, FWNWHHFKG-, IKIFFFSFG-, and FFNFFKG-Toyopearl resins (Supporting Information: Figure S16).

All measurements were conducted at the residence time (RT) of 3 min, which is recommended for both POROS™ AAVX and AVB Sepharose resins (Cytiva; Thermo Scientific™. POROS™ Capture-Select™ AAV Resins: AAV8, AAV9, AAVX) (note: AAV2 capsids labeled with a green fluorescent dye (AlexaFluor 488) were loaded in a column packed with KFNHWF-Toyopearl resins at the RT of 3 min; the images the beads obtained via fluorescence confocal microscopy (Supporting Information: Figure S17) demonstrate that the AAVs can penetrate the resin beads). The values of DBC_{10%} reported in Table 2 met the value of 10¹³ viral particles/mL of resin—regarded by the community as the standard for affinity resins intended for AAV purification—thus supporting the adoption of peptides ligands for the product capture step in virus biomanufacturing.

3 | DISCUSSION

Viral vectors—and, chiefly among them, AAVs—are poised to become the focus of next-generation treatment of rare cardiovascular, muscular, neurological, and ophthalmological diseases. Following the approval of LUXTURNA® (AAV9) for the treatment of retinal dystrophy (2019) and ZOLGENSMA® (AAV2) for treating pediatric patients with spinal muscular atrophy, late in 2022, The US FDA approved CSL's HEMGENIX®, an AAV5-based gene therapy for hemophilia B. With the expected uptick in regulatory approvals and the exponential growth of the clinical trials adsorbents on viral vector-based gene therapies poses a defined need for affordable tools for manufacturing AAV-based therapies, which currently carry price tags over \$2.5 M. In this context, a key role will be played by purification technology and particularly by affinity adsorbents for universal AAV purification. The adsorbents currently in the market have drawn substantially—both in the morphology of the beads and the design of the ligands—from the Protein A adsorbents employed in antibody purification, and are therefore poorly suited for AAV purification. Responding to these challenges, this study presented the development of the first set of serotype-agnostic AAV-targeting peptide ligands. The use of synthetic peptide ligands is particularly apt to the purification of viral vectors, since it (i) enables promiscuous targeting of conserved epitopes on the surface of the AAV capsids while ensuring sufficient selectivity to afford a significant reduction of process-related impurities; and (ii) features a moderate binding strength, thus enabling efficient elution of the bound capsids under near-physiological conditions, which are much milder than those requires for commercial affinity resins and afford an AAV product with superior transduction activity. The combination of universal serotype targeting, high binding capacity, excellent purification activity, and safeguarding the capsid's transduction activity at a fraction of the cost of commercial adsorbents make these peptide-based adsorbents valuable tools for large-scale applications supporting clinical efforts. Future studies on the peptides introduced in this work will aim at optimizing the (i) design of the peptide-functionalized adsorbents—focusing on substrate material, resin bead diameter and pore diameter, and ligand density—to increase binding capacity, since

we anticipate that larger pores (e.g., ~1000 nm as found in POROS™ resins) may facilitate the access of AAVs to the resin beads; and the (ii) the concentration of MgCl₂ needed to elute the various AAV serotypes, since the differences in the amino acid sequence of the VP proteins across different serotypes are likely to result in a different response of the AAV:peptide complex to the elution buffer, and thus different product release. Finally, the workflow developed in this study will soon be extended to other viral vectors of medicinal relevance, such as lentivirus and adenovirus.

4 | MATERIALS AND METHODS

4.1 | Materials

Aminomethyl ChemMatrix (particle size: 100–200 mesh; primary amine density: 0.5–0.7 mmol/g) resins were sourced from PCAS Biomatrix, Inc. (Saint-Jean-sur-Richelieu). The Toyopearl AF-Amino-650M resin (pore size: 100 nm; particle size: 65 μm; ligand density: 250 μmol/mL resin) was obtained from Tosoh Corporation. Fluorenylmethoxycarbonyl- (Fmoc-) protected amino acids Fmoc-Ser(tBu)-OH, Fmoc-Ile-OH, Fmoc-Phe-OH, Fmoc-Trp(Boc)-OH, Fmoc-His(Trt)-OH, Fmoc-Ala-OH, Fmoc-Asn(Trt)-OH, Fmoc-Lys(Boc)-OH, Fmoc-Glu(OtBu)-OH, and Fmoc-Gly-OH, Hexafluorophosphate Azabenzotriazole Tetramethyl Uronium (HATU), piperidine, diisopropylethylamine (DIPEA), and trifluoroacetic acid (TFA) were obtained from ChemImpex International. Triisopropylsilane (TIPS), Kaiser test kits, 1,2-ethanedithiol (EDT), polybrene, and PBS at pH 7.4 were obtained from MilliporeSigma. NHS-Alexa Fluor 594 (NHS-AF594) and NHS-Alexa Fluor 488 (NHS-AF488), *N*-methyl-2-pyrrolidone (NMP), *N,N'*-dimethylformamide (DMF), dichloromethane (DCM), methanol, POROS™ CaptureSelect™ AAVX Affinity Resin, Pluronic™ F-68 Non-ionic Surfactant, SilverQuest™ Silver Staining Kit, hydrochloric acid (HCl), sodium hydroxide (NaOH), potassium chloride (KCl), sodium chloride (NaCl), magnesium chloride (MgCl₂), and Bis-Tris HCl were obtained from Fisher Chemical. Dulbecco's modified Eagle medium (DMEM) and fetal bovine serum (FBS) were sourced from ThermoFisher. Human fibrosarcoma (HT1080) cells were obtained from ATCC. The AVB Sepharose HP was sourced from Cytiva. Clarified HEK 293 cell lysates containing AAV2, and null HEK 293 cell culture lysate were donated by BTEC. All chromatographic experiments were performed using an ÄKTA Avant system from Cytiva. Alltech chromatography columns (diameter: 3.6 mm; length: 50 mm; volume: 0.5 mL), and 10 μm polyethylene frits were obtained from VWR International. A BioResolve SEC mAb Column (particle diameter: 2.5 μm; pore diameter: 200 Å; column diameter: 7.8 mm; column length: 300 mm) SEC column was obtained from Waters Inc. A CIMac OH 0.1 mL analytical monolith column (diameter: 5.2 mm; length: 4.95 mm; volume: 0.1 mL, channel radius: 2 μm) for SXC analysis was obtained from BIA Separations (Ajdovščina, Slovenia). The 10%–20% Tris-Glycine HCl sodium dodecyl sulfate-polyacrylamide gel electrophoresis (SDS-PAGE) gels were purchased from Bio-Rad Life Sciences. The AAV ELISA kits

were purchased from Progen, while the HEK 293 ELISA kits were purchased from Cygnus.

4.2 | Synthesis of peptide libraries on aminomethyl-ChemMatrix resin and selected peptides on Toyopearl resin

Peptide synthesis was performed on a Syro I automated peptide synthesizer (Biotage) using nine protected amino acids, namely Fmoc-Ser(tBu)-OH, Fmoc-Ile-OH, Fmoc-Phe-OH, Fmoc-Trp(Boc)-OH, Fmoc-His(Trt)-OH, Fmoc-Ala-OH, Fmoc-Asn(Trt)-OH, Fmoc-Lys(Boc)-OH, and Fmoc-Glu(OtBu)-OH (Chu et al., 2022; Kilgore et al., 2023). Each amino acid coupling step was performed at 45°C for 20 min, using three equivalents (eq.) of protected amino acid at the concentration of 0.5 M, 3 eq. of HATU and 0.5 M, 6 eq. of DIPEA (0.5 M) in 5 mL of dry DMF. The yield of peptide conjugation was monitored after each amino acid via the Kaiser test. The removal of Fmoc protecting groups was performed at room temperature using 20% piperidine in DMF. The 6-mer (X₁-X₂-X₃-X₄-X₅-X₆) and 8-mer (X₁-X₂-X₃-X₄-X₅-X₆-X₇-X₈) peptide libraries were synthesized on 2 g of Aminomethyl-ChemMatrix resin preloaded with the tripeptide spacer GSG (G: glycine; S: serine) following the “split-couple-recombine” method (Chu et al., 2022; Lam et al., 1991, 1993, 1996). Selected peptides IWWHIAKF, FWNWHHFK, FWWAAFFK, IAFKKI-SI, IKIFFFFS, GYISRHPG, KFNHWF, WKAHNK, KWWIWA, WWIKIS, FFNFFK, and FNHFFI were synthesized on Toyopearl AF-Amino-650M resin at the density of ~0.12–0.15 mmol of peptide per gram of resin (*note*: minor sequence-dependent variability in peptide density is expected). Upon completing chain elongation, the peptides were deprotected via acidolysis using a cleavage cocktail containing TFA, thioanisole, anisole, and EDT (94/3/2/1) for 2 h. After deprotection, the ChemMatrix library resins were rinsed with DCM and DMF and stored in DMF at 4°C, whereas the peptide-Toyopearl resins were washed sequentially with DCM, DMF, methanol, and stored in 20% v/v aqueous methanol.

4.3 | Fluorescent labeling of AAV and HEK 293 HCPs

The labeling method of viral vector and proteins was performed as reported in the previous studies (Chu et al., 2022; Prodromou et al., 2021). The AAV2, AAV9 were labeled using NHS-Alexafluor 594 (NHS-AF594, red), while the HCPs contained in the HEK 293 cell culture lysate were collectively labeled with NHS-Alexafluor 488 (NHS-AF488, green). Both dyes were initially dissolved in anhydrous DMSO to a concentration of 10 mg/mL. A volume of 1 µL of NHS-AF594 was added to 100 µL of AAV solution at 10¹³ vp/mL in PBS pH 7.4, while 200 µL of NHS-AF488 was added to 4 mL of null HEK 293 cell culture lysate at the HCP titer of 300 µg/mL. The labeling reactions were allowed to proceed for 1 h at room temperature, under dark and gentle agitation. The unreacted dyes were removed

using 0.5 mL Zeba™ Dye and Biotin Removal Spin Columns (ThermoFisher Scientific). The concentration of the labeled AAV2 and AAV9 in solution was determined by AAV ELISA assay and the concentration of the labeled proteins in solution was determined by Bradford assay. The absorbance of the solutions of AF488-labeled HEK 293 HCPs and AF594-labeled AAV was measured by UV spectrophotometry at the wavelength of 490 and 590 nm, respectively, using a Synergy H1 plate reader (Biotek).

4.4 | Dual-fluorescence screening of peptide library against AAV in HEK 293 cell culture lysate

The screening process of AAV-targeting peptides was performed as reported in the previous studies (Chu et al., 2022; Prodromou et al., 2021). A screening mix was initially prepared by spiking AF594-labeled AAV2 and AAV9 in AF488-labeled HEK 293 cell culture lysate to obtain a final AAV titer of 5 × 10¹¹ vp/mL and a HEK 293 HCP titer of ~0.5 mg/mL. Aliquots of 10 µL of library beads were initially equilibrated with PBS at pH 7.4 and subsequently incubated with 40 µL of screening mix for 2 h at room temperature in the dark. The beads were thoroughly washed with PBS at pH 7.4 and 0.1% v/v Tween 20 in PBS at pH 7.4 and sorted automatically using the microfluidic screening device developed in prior work (Day et al., 2019; Prodromou et al., 2021; Saberi-Bosari et al., 2019). The beads were fed to the microfluidic sorter, which is controlled by a custom-made MATLAB code programmed to discard the nonfluorescent, the green-only, and red-and-green beads, and withhold beads with strong red-only fluorescence. The latter were exposed to a flow of 1 M MgCl₂ in 20 mM Bis-Tris HCl buffer at pH 6.0 for 2 min at room temperature. Every bead that displayed a measurable loss of red fluorescence was selected as a positive lead, individually incubated with 100 µL of 0.1 M glycine buffer at pH 2.5 for 1 h at room temperature in the dark to elute the bound AF594-labeled AAV, and rinsed with Milli-Q water and acetonitrile. The beads were finally analyzed via Edman degradation using a PPSQ-33A protein sequencer (Shimadzu) to identify the peptide sequences carried thereupon.

4.5 | Static binding capacity and affinity of AAV2 on KFNHWF-Toyopearl resins

Aliquots of 50 µL of KFNHWF-Toyopearl resin were transferred in a tube, swollen in 20% v/v aqueous ethanol, washed in MilliQ water, and equilibrated in PBS at pH 7.4. The resin aliquots were incubated with 0.5 mL of a solution of AAV2 at different titers—namely, 2.9 × 10¹¹, 3.6 × 10¹¹, 4.8 × 10¹¹, 7.2 × 10¹¹, 1.4 × 10¹², 2.9 × 10¹², and 5.8 × 10¹² vp/mL—for 1.5 h at room temperature under gentle rotation. After incubation, the resin aliquots were centrifuged and the UB fraction was collected; the resins were then washed with 0.5 mL of PBS for 30 min and the supernatants were combined with the corresponding UB fractions. These were finally analyzed via

AAV2-specific ELISA Kit to measure the concentrations of AAV2 in solution at the equilibrium with the resin (C^*), from which the values of bound AAV2 per volume of resin (q) were determined by mass balance. The values of q versus C^* were plotted and fit using a Langmuir isotherm (Equation 1) to determine the maximum binding capacity (Q_{\max}) and dissociation constant (K_D).

$$q = \frac{Q_{\max} \cdot C^*}{K_D + C^*} \quad (1)$$

4.6 | Dynamic binding capacity of peptide-Toyopearl resins

The dynamic binding capacity at 10% breakthrough ($DBC_{10\%}$, vp/mL resin) of peptide-Toyopearl resins were measured as reported in prior studies (Chu et al., 2022; Reese et al., 2020; Wang et al., 2016). A volume of 0.5 mL of resin packed in an Alltech chromatography column was initially washed with 10 column volumes (CVs) of 20% v/v ethanol and deionized water (3 CVs) and equilibrated with 10 CVs of PBS buffer. A volume of 30 mL of solution of AAV2 at 3.2×10^{11} vp/mL in HEK 293 lysate (HCP titer ~ 0.5 mg/mL) was loaded on the column at the flow rate of 0.17 mL/min (RT: 3 min). The resin was then washed with 20 CVs of binding buffer at 0.5 mL/min. The AAV elution from the peptide-Toyopearl resins was performed using 1 M $MgCl_2$ in 20 mM Bis-Tris HCl buffer at pH 6.0 at the flow rate of 0.25 mL/min (RT: 2 min); as recommended by manufacturers, elution from POROS™ CaptureSelect™ AAVX affinity resin and AVB Sepharose HP resin was performed at the flow rate of 0.25 mL/min (RT: 2 min) using 0.2 M $MgCl_2$ in 200 mM citrate buffer at pH 2.2 and PBS at pH 2.0, respectively. All resins were regenerated with 10 CVs of PBS buffer at pH 2.0 at the flow rate of 0.5 mL/min. The effluents from flowthrough step were continuously monitored by UV spectrometry at 280 nm and collected in volume of 1 mL/tube. The collected fractions were analyzed by AAV ELISA Kit to generate the breakthrough curves, and the resulting chromatograms were utilized to calculate the $DBC_{10\%}$.

4.7 | Purification of AAV from HEK 293 cell culture lysate using peptide-Toyopearl resins

Each peptide-functionalized resin and commercial resins was individually wet packed in the 0.5 mL Alltech column, washed with 20% v/v ethanol (10 CVs) and deionized water (3 CVs), and equilibrated with 10 CVs of 20 mM NaCl in 20 mM Bis-Tris HCl buffer at pH 7.0. A volume of 12 mL of AAV2 at $\sim 1.6 \times 10^{11}$ vp/mL in HEK 293 cell culture lysate (HCP titer ~ 0.5 mg/mL) was loaded on the column at the flow rate of 0.17 mL/min (RT: 3 min). Following load, the resin was washed with binding buffer (20 CVs) to recover the UV_{280nm} baseline. The AAV elution from the peptide-Toyopearl resins was performed using 1 M $MgCl_2$ in 20 mM Bis-Tris HCl buffer at pH 6.0 at the flow rate of 0.25 mL/min (RT: 2 min); elution from POROS™ CaptureSelect™

AAVX affinity resin and AVB Sepharose HP resin was performed at the flow rate of 0.25 mL/min (RT: 2 min) using 0.2 M $MgCl_2$ in 200 mM citrate buffer at pH 2.2 and PBS at pH 2.0, respectively. All resins were regenerated with 10 CVs of PBS buffer at pH 2.0 at the flow rate of 0.5 mL/min. The IKIFFFS-Toyopearl resin was also cleaned with aqueous 0.5 M NaOH and utilized for five successive cycles of AAV2 purification. The collected flow-through and elution fractions were analyzed by AAV2 ELISA Kit (see Section 4.8) and qPCR (see Section 4.9) to measure the titer of AAV2 particles and viral genome, respectively, and determine the values of product yield and full:empty capsid ration; HEK 293 ELISA Kit (see Section 4.10), SEC (see Section 4.11), SXC (see Section 4.12), gel electrophoresis (see Section 4.13) to determine the values of product purity, and FFC (see Section 4.14) to quantify the transduction efficiency of the eluted AAVs.

4.8 | Quantification of AAV viral particle via ELISA

The titer of AAV particles in the feedstock, flow-through, and elution fractions collected as described in Sections 4.6 and 4.7 was measured using an AAV Titration ELISA kit (PROGEN) following the manufacturer's protocol. The total capsids of AAV adsorbed per volume of resin were calculated via mass balance.

4.9 | Quantification of viral genomes via qPCR

The collected chromatographic fractions were initially treated with TurboDNase followed by RNA isolation using a Purelink Viral RNA/DNA Kit (ThermoFisher Scientific). The samples were then combined with TaqMan fast virus, custom TaqMan probe, and the primers listed in Table 3, and analyzed using a CFX Duet Real-Time qPCR System (Bio-Rad).

4.10 | Quantification of HEK 293 HCPs

The titer of HEK 293 HCPs in the feedstock, flow-through, and elution fractions collected as described in Section 4.7 were determined using a HEK 293 HCP ELISA kit (Cygnus Technologies) following the manufacturer's protocol. The values of HCP LRV in the effluents were calculated via mass balance.

TABLE 3 Primers and probe sequences for the quantification of viral genome via qPCR.

Primer	DNA sequence
Forward primer	CCCAGTTCGCCATTCTC
Reverse primer	GCCTCGGCTCTGCATAAATAAA
Probe	ATGGCTGACTAATTTTT

Abbreviation: qPCR, quantitative polymerase chain reaction.

4.11 | Qualification of AAV purity by SEC

The feedstock, and the flow-through and elution fractions collected as described in Section 4.7 were analyzed by analytical SEC using a BioResolve SEC mAb Column (Waters) operated with a 40-min isocratic method using 200 mM KCl in 50 mM sodium phosphate at pH 7.0 (0.05% v/v sodium azide) as mobile phase. A volume of 10 μ L of sample was injected and the effluent continuously monitored via UV (abs: 260 and 280 nm) fluorescence spectroscopy (ex/em: 280/350 nm).

4.12 | Qualification of AAV purity by SXC

The feedstock, the flow-through, and elution fractions collected as described in Section 4.7 were analyzed by analytical SXC using a monolith CIMac OH 0.1 mL analytical column (BIA separations) operated with a 20-min linear gradient from 100:0 A:B to 0:100 A:B at the flow rate of 0.33 mL/min (mobile phase A: PBS at pH 7.0 added with 10% v/v PEG 6 K; mobile phase B: 3 \times PBS at pH 7.0). Injection volumes were normalized via AAV ELISA titer to compare each elution condition and the effluent continuously monitored via fluorescence spectroscopy (ex/em: 280/350 nm) (Greback-Clarke, 2023).

4.13 | Quantification of AAV purity by SDS-PAGE

The feedstock, the flow-through, and elution fractions collected as described in Section 4.7 were analyzed by reducing SDS-PAGE using 4-20% Mini-PROTEAN™ TGX™ Precast protein gels (Bio-Rad) and 1 \times Tris/Glycine/SDS Buffer (Bio-Rad) as running buffer. A volume of 40 μ L of sample, each adjusted to a total AAV titer of $\sim 1 \times 10^{12}$ vp/mL, was loaded to the wells of SDS-PAGE gels. The sample stripes were concentrated under 80 V for about 30 min and separated under 120 V for about 1 h. The gels were then stained using a SilverQuest™ Silver Staining Kit (ThermoFisher) and finally imaged by the Gel Doc2000 imaging system (Bio-Rad).

4.14 | Quantification of AAV transduction efficiency via FFC

HT1080 cells were cultured in DMEM media supplemented with 10% v/v FBS at 5% CO₂ and 37°C. Upon reaching 80%–90% confluence, cells were seeded in 96-well plates at a density of 6000 cells/well and cultured overnight. The eluted fractions containing AAVs were serially diluted in DMEM medium (without FBS and antibiotics) added with polybrene at 8 μ g/mL, and 0.1 mL of diluted AAV sample was incubated with the HT1080 cells in the 96-well plates. After 24 h, spent medium was replaced with fresh DMEM containing FBS and the cells were cultured for 3 days. The percentage of cells expressing GFP (GFP⁺) was quantified using a CytoFlex flow

cytometer (Beckman Coulter) and the number of transduction units per mL (TU/mL) was calculated using Equation 2:

$$\text{Activity} \left(\frac{\text{TU}}{\text{mL}} \right) = \frac{N_{\text{HT1080}} \times \% \text{GFP}^+}{V \times DF}, \quad (2)$$

wherein N_{HT1080} is the number of cells incubated with each diluted AAV sample, V is the volume of the diluted AAV sample, and DF is the dilution factor.

4.15 | In silico identification of putative peptide binding sites on AAV and analysis of AAV: peptide complexes

The crystal structures of AAV2 and AAV9 were initially prepared using Protein Prep Wizard (PPW; Schrödinger) (Madhavi Sastry et al., 2013) by correcting missing atoms and side chains, removing salt ions, adding explicit hydrogens, and optimizing the hydrogen-bonding network. Four clusters, each comprising 15 virion proteins—namely, one VP1, one VP2, and thirteen VP3 to recapitulate the $\sim 1:1:10$ ratio reported for AAV capsids (Stagg et al., 2022; Wang et al., 2019)—and arranged in a spherical cap that represents $\frac{1}{4}$ of the capsid surface were obtained from the Protein DataBank for AAV2 (PDB IDs: 6U0V, 6IH9, 5IPI, and 6IHB) and AAV9 (3UX1, 7MT0, 7WJW, and 7WJX). The ionization states at pH 7.4 and pH 6.0, and the corresponding structural minimization of the eight VP clusters were performed using PROPKA (Olsson et al., 2011; Rostkowski et al., 2011). The adjusted structure was then analyzed using SiteMap to identify sites for peptide binding (Halgren, 2007, 2009; Sharma et al., 2020) and the sites with high S-score (>0.8) and D-score (>0.9) were selected for peptide docking. The AAV2:antibody complex (3J1S) and the AAV9:AAVR complex (7WJX) were utilized as reference structures. Peptides IWWHIAKF, FWNWVHFK, FWWAAFFK, IAFKKISI, IKIFFFFS, GYISRHGP, KFNHWF, WKAHNNK, KWWIWA, WWIKIS, FFNFFK, and FNHFFI were constructed using the molecular editor Avogadro (Hanwell et al., 2012) and their structures were simulated in GROMACS using the GROMOS 43a1 force field. Briefly, each peptide was initially placed in a simulation box with periodic boundary containing 1000 TIP3P water molecules and equilibrated with 10,000 steps of steepest gradient descent; and heated to 300 K in an NVT ensemble for 250 ps using 1 fs time steps, and equilibrated to 1 atm via a 500-ps NPT simulation with 2 fs time steps. Production runs were then performed in the NPT ensemble at 300 K and 1 atm using the Nosé–Hoover thermostat and the Parrinello–Rahman barostat (Kleinerman et al., 2008; Parrinello & Rahman, 1981); the leap-frog algorithm with integration steps of 2 fs was used to integrate the motion equations; the covalent bonds were constrained using the LINCS algorithm, the Lennard–Jones, and short-range electrostatic interactions were calculated using cut-off values of 1.0 and 1.4 nm, respectively, while the particle-mesh Ewald method was utilized for long-range electrostatic interactions (Cheatham et al., 1995); the lists of bonded and nonbonded interactions (cutoff of 1.4 nm) were updated every 2 and 5 fs,

respectively. The energetic landscape associated to the various peptide conformations was sampled to identify the structures with absolute energy minima. The selected peptide ligands were then docked in silico against the putative binding sites on AAV2 and AAV9 using the docking software HADDOCK (High Ambiguity Driven Protein-Protein Docking, v.2.4) (Honorato et al., 2021; van Zundert et al., 2016). The residues on the selected binding sites of AAV2 and AAV9, and the X₁-X₂-X₃-X₄-X₅-X₆(-X₇-X₈) residues on the peptides were marked as “active,” while the surrounding residues were marked as “passive.” The docked AAV:peptide structures were grouped in clusters of up to 20 complexes based on Ca root mean square deviation < 7.5 Å and ranked using the dampened molecular mechanics poisson-boltzmann surface area score (Spiliotopoulos et al., 2016). Finally, the top AAV:peptide complexes were refined via 150-ns atomistic MD simulations and evaluated to estimate the free energy of binding (ΔG_B).

AUTHOR CONTRIBUTIONS

Wenning Chu, Shriarjun Shastry, Eduardo Barbieri, Raphael Prodromou, Paul Greback-Clarke, Will Smith, Brandyn Moore, Ryan Kilgore, and Christopher Cummings conducted the experimental work. Wenning Chu, Jennifer Pancorbo, Gary Gilleskie, Michael A. Daniele, and Stefano Menegatti conceived the work and wrote the manuscript.

ACKNOWLEDGMENTS

The authors wish to acknowledge the funding provided by the National Science Foundation (CBET 1743404 and CBET 1653590), the Novo Foundation (AIM-Bio Grant NNF19SA0035474), the Food and Drug Administration (Grant R01FD007481) as well as the generous support of the Golden LEAF Biomanufacturing Training and Education Center (BTEC) and the North Carolina Viral Vector Initiative in Research and Learning (NC-VVIRAL) at NC State University.

CONFLICT OF INTEREST STATEMENT

The authors declare no conflict of interest.

DATA AVAILABILITY STATEMENT

The data that support the findings of this study are available from the corresponding author upon reasonable request.

ORCID

Wenning Chu  <https://orcid.org/0000-0002-6033-0963>

Gary Gilleskie  <http://orcid.org/0000-0002-5016-6370>

Stefano Menegatti  <http://orcid.org/0000-0001-5633-434X>

REFERENCES

AAV Serotypes and AAV Tissue-specific Tropism. <https://www.genemedi.net/i/aav-serotypes-tissue-specific-tropism>

Adams, B., Bak, H., & Tustian, A. D. (2020). Moving from the bench towards a large scale, industrial platform process for adeno-associated viral vector purification. *Biotechnology and Bioengineering*, 117, 3199–3211. <https://doi.org/10.1002/bit.27472>

Aina, O. H., Liu, R., Sutcliffe, J. L., Marik, J., Pan, C.-X., & Lam, K. S. (2007). From combinatorial chemistry to cancer-targeting peptides. *Molecular Pharmaceutics*, 4, 631–651. <https://doi.org/10.1021/mp700073y>.

Asokan, A., Conway, J. C., Phillips, J. L., Li, C., Hegge, J., Sinnott, R., Yadav, S., DiPrimio, N., Nam, H.-J., Agbandje-McKenna, M., McPhee, S., Wolff, J., & Samulski, R. J. (2010). Reengineering a receptor footprint of adeno-associated virus enables selective and systemic gene transfer to muscle. *Nature Biotechnology*, 28, 79–82.

Asokan, A., Schaffer, D. V., & Jude Samulski, R. (2012). The AAV vector toolkit: Poised at the clinical crossroads. *Molecular Therapy*, 20, 699–708.

AVIPure®—AAV Affinity Resins. <https://www.repligen.com/technologies/resins/aav-affinity-resins>

Barozzi, A., Lavoie, R. A., Day, K. N., Prodromou, R., & Menegatti, S. (2020). Affibody-binding ligands. *International Journal of Molecular Sciences*, 21, 3769. <https://doi.org/10.3390/ijms21113769>.

Blessing, D., Vachey, G., Pythoud, C., Rey, M., Padrun, V., Wurm, F. M., Schneider, B. L., & Déglon, N. (2019). Scalable production of AAV vectors in orbitally shaken HEK293 cells. *Molecular Therapy: Methods & Clinical Development*, 13, 14–26.

Borrel, A., Regad, L., Xhaard, H., Petitjean, M., & Camproux, A.-C. (2015). PockDrug: A model for predicting pocket druggability that overcomes pocket estimation uncertainties. *Journal of Chemical Information and Modeling*, 55, 882–895.

Chamberlain, K., Riyad, J. M., & Weber, T. (2016). Expressing transgenes that exceed the packaging capacity of adeno-associated virus capsids. *Human Gene Therapy Methods*, 27, 1–12.

Cheatham, III, T. E. I., Miller, J. L., Fox, T., Darden, T. A., & Kollman, P. A. (1995). Molecular dynamics simulations on solvated biomolecular systems: The particle mesh ewald method leads to stable trajectories of DNA, RNA, and proteins. *Journal of the American Chemical Society*, 117, 4193–4194. <https://doi.org/10.1021/ja00119a045>.

Chu, W., Prodromou, R., Moore, B., Elhanafi, D., Kilgore, R., Shastry, S., & Menegatti, S. (2022). Development of peptide ligands for the purification of α -1 antitrypsin from cell culture fluids. *Journal of Chromatography A*, 1679, 463363.

Clark, K. R., Liu, X., McGrath, J. P., & Johnson, P. R. (1999). Highly purified recombinant adeno-associated virus vectors are biologically active and free of detectable helper and wild-type viruses. *Human Gene Therapy*, 10, 1031–1039.

Clément, N., & Grieger, J. C. (2016). Manufacturing of recombinant adeno-associated viral vectors for clinical trials. *Molecular Therapy: Methods & Clinical Development*, 3, 16002.

Cytiva. AVB sepharose high performance. <https://www.cytivalifesciences.com/en/us/shop/chromatography/resins/affinity-specific-groups/avb-sepharose-high-performance-p-05953>

Das, S. K., Menezes, M. E., Bhatia, S., Wang, X.-Y., Emdad, L., Sarkar, D., & Fisher, P. B. (2015). Gene therapies for cancer: Strategies, challenges and successes. *Journal of Cellular Physiology*, 230, 259–271. <https://doi.org/10.1002/jcp.24791>

Day, K., Prodromou, R., Saberi Bosari, S., Lavoie, A., Omary, M., Market, C., San Miguel, A., & Menegatti, S. (2019). Discovery and evaluation of peptide ligands for selective adsorption and release of Cas9 nuclease on solid substrates. *Bioconjugate Chemistry*, 30, 3057–3068. <https://doi.org/10.1021/acs.bioconjchem.9b00703>

Day, K., Schneible, J. D., Young, A. T., Pozdin, V. A., Van Den Driessche, G., Gaffney, L. A., Prodromou, R., Freytes, D. O., Fourches, D., Daniele, M., & Menegatti, S. (2020). Photoinduced reconfiguration to control the protein-binding affinity of azobenzene-cyclized peptides. *Journal of Materials Chemistry B*, 8, 7413–7427. <https://doi.org/10.1039/D0TB01189D>.

DiMattia, M. A., Nam, H.-J., Van Vliet, K., Mitchell, M., Bennett, A., Gurda, B. L., McKenna, R., Olson, N. H., Sinkovits, R. S., Potter, M.,

- Byrne, B. J., Aslanidi, G., Zolotukhin, S., Muzyczka, N., Baker, T. S., & Agbandje-McKenna, M. (2012). Structural insight into the unique properties of adeno-associated virus serotype 9. *Journal of Virology*, *86*, 6947–6958.
- Drouin, L. M., & Agbandje-McKenna, M. (2013). Adeno-associated virus structural biology as a tool in vector development. *Future Virology*, *8*, 1183–1199.
- Eisenman, D. (2019). The United States' regulatory environment is evolving to accommodate a coming boom in gene therapy research. *Applied Biosafety*, *24*, 147–152. <https://doi.org/10.1177/1535676019854866>
- Fumagalli, F., Calbi, V., Natali Sora, M. G., Sessa, M., Baldoli, C., Rancoita, P. M. V., Ciotti, F., Sarzana, M., Frascini, M., Zambon, A. A., Acquati, S., Redaelli, D., Attanasio, V., Miglietta, S., De Mattia, F., Barzagli, F., Ferrua, F., Migliavacca, M., Tucci, F., ... Aiuti, A. (2022). Lentiviral haematopoietic stem-cell gene therapy for early-onset metachromatic leukodystrophy: Long-term results from a non-randomised, open-label, phase 1/2 trial and expanded access. *The Lancet*, *399*, 372–383.
- Gao, G., Vandenberghe, L., & Wilson, J. (2005). New recombinant serotypes of AAV vectors. *Current Gene Therapy*, *5*, 285–297.
- Gao, G., Vandenberghe, L. H., Alvira, M. R., Lu, Y., Calcedo, R., Zhou, X., & Wilson, J. M. (2004). Clades of adeno-associated viruses are widely disseminated in human tissues. *Journal of Virology*, *78*, 6381–6388.
- Giles, A. R., Sims, J. J., Turner, K. B., Govindasamy, L., Alvira, M. R., Lock, M., & Wilson, J. M. (2018). Deamidation of amino acids on the surface of adeno-associated virus capsids leads to charge heterogeneity and altered vector function. *Molecular Therapy*, *26*, 2848–2862. <https://doi.org/10.1016/j.ymthe.2018.09.013>
- Ginn, S. L., Amaya, A. K., Alexander, I. E., Edelstein, M., & Abedi, M. R. (2018). Gene therapy clinical trials worldwide to 2017: An update. *The Journal of Gene Medicine*, *20*:e3015.
- Greback-Clarke, P. (2023). Quantification of AAV particles by steric exclusion chromatography (SXC-HPLC) [Master's thesis, North Carolina State University]. NC State University Repository. <https://www.lib.ncsu.edu/resolver/1840.20/nnnm>
- Grieger, J. C., Soltys, S. M., & Samulski, R. J. (2016). Production of recombinant adeno-associated virus vectors using suspension HEK293 cells and continuous harvest of vector from the culture media for GMP FIX and FLT1 clinical vector. *Molecular Therapy*, *24*, 287–297. <https://doi.org/10.1038/mt.2015.187>
- Hagen, S., Baumann, T., Wagner, H. J., Morath, V., Kaufmann, B., Fischer, A., Bergmann, S., Schindler, P., Arndt, K. M., & Müller, K. M. (2014). Modular adeno-associated virus (rAAV) vectors used for cellular virus-directed enzyme prodrug therapy. *Scientific Reports*, *4*, 3759.
- Halgren, T. (2007). New method for fast and accurate binding-site identification and analysis. *Chemical Biology & Drug Design*, *69*, 146–148. <https://doi.org/10.1111/j.1747-0285.2007.00483.x>
- Halgren, T. A. (2009). Identifying and characterizing binding sites and assessing druggability. *Journal of Chemical Information and Modeling*, *49*, 377–389. <https://doi.org/10.1021/ci800324m>
- Hanwell, M. D., Curtis, D. E., Lonie, D. C., Vandermeersch, T., Zurek, E., & Hutchison, G. R. (2012). Avogadro: An advanced semantic chemical editor, visualization, and analysis platform. *Journal of Cheminformatics*, *4*, 17. <https://doi.org/10.1186/1758-2946-4-17>
- Hinderer, C., Katz, N., Buza, E. L., Dyer, C., Goode, T., Bell, P., Richman, L. K., & Wilson, J. M. (2018). Severe toxicity in nonhuman primates and piglets following high-dose intravenous administration of an adeno-associated virus vector expressing human SMN. *Human Gene Therapy*, *29*, 285–298.
- Honorato, R. V., Koukos, P. I., Jiménez-García, B., Tsaregorodtsev, A., Verlato, M., Giachetti, A., Rosato, A., & Bonvin, A. M. J. J. (2021). Structural biology in the clouds: The WeNMR-EOSC ecosystem. *Frontiers in Molecular Biosciences*, *8*. <https://doi.org/10.3389/fmolb.2021.729513>.
- Hussein, H. A., Borrel, A., Geneix, C., Petitjean, M., Regad, L., & Camproux, A.-C. (2015). PockDrug-server: A new web server for predicting pocket druggability on holo and apo proteins. *Nucleic Acids Research*, *43*, W436–W442.
- Kaludov, N., Handelman, B., & Chiorini, J. A. (2002). Scalable purification of adeno-associated virus type 2, 4, or 5 using ion-exchange chromatography. *Human Gene Therapy*, *13*, 1235–1243. <https://doi.org/10.1089/104303402320139014>
- Kaplitt, M. G., Feigin, A., Tang, C., Fitzsimons, H. L., Mattis, P., Lawlor, P. A., Bland, R. J., Young, D., Strybing, K., Eidelberg, D., & During, M. J. (2007). Safety and tolerability of gene therapy with an adeno-associated virus (AAV) borne GAD gene for parkinson's disease: An open label, phase I trial. *The Lancet*, *369*, 2097–2105.
- Keeler, A. M., & Flotte, T. R. (2019). Recombinant adeno-associated virus gene therapy in light of Luxturna (and Zolgensma and Glybera): Where are we, and how did we get here? *Annual Review of Virology*, *6*, 601–621.
- Kilgore, R., Chu, W., Bhandari, D., Fischler, D., Carbonell, R. G., Crapanzano, M., & Menegatti, S. (2023). Development of peptide affinity ligands for the purification of polyclonal and monoclonal Fabs from recombinant fluids. *Journal of Chromatography A*, *1687*, 463701. <https://doi.org/10.1016/j.chroma.2022.463701>
- Kish, W. S., Sachi, H., Naik, A. D., Roach, M. K., Bobay, B. G., Blackburn, R. K., Menegatti, S., & Carbonell, R. G. (2017). Design, selection, and development of cyclic peptide ligands for human erythropoietin. *Journal of Chromatography A*, *1500*, 105–120. <https://doi.org/10.1016/j.chroma.2017.04.019>
- Kleinerman, D. S., Czaplewski, C., Liwo, A., & Scheraga, H. A. (2008). Implementations of Nosé-Hoover and Nosé-Poincaré thermostats in mesoscopic dynamic simulations with the united-residue model of a polypeptide chain. *The Journal of Chemical Physics*, *128*, 245103. <https://doi.org/10.1063/1.2943146>
- Lai, Y., Yue, Y., & Duan, D. (2010). Evidence for the failure of adeno-associated virus serotype 5 to package a viral genome \geq 8.2 kb. *Molecular Therapy*, *18*, 75–79.
- Lam, K. S., Hruby, V. J., Lebl, M., Knapp, R. J., Kazmierski, W. M., Hersh, E. M., & Salmon, S. E. (1993). The chemical synthesis of large random peptide libraries and their use for the discovery of ligands for macromolecular acceptors. *Bioorganic & Medicinal Chemistry Letters*, *3*, 419–424. [https://doi.org/10.1016/S0960-894X\(01\)80224-9](https://doi.org/10.1016/S0960-894X(01)80224-9)
- Lam, K. S., Lake, D., Salmon, S. E., Smith, J., Chen, M. L., Wade, S., Abdul-Latif, F., Knapp, R. J., Leblova, Z., Ferguson, R. D., Krchnak, V., Sepetov, N. F., & Lebl, M. (1996). A one-bead one-peptide combinatorial library method for B-cell epitope mapping. *Methods*, *9*, 482–493. <https://doi.org/10.1006/meth.1996.0056>
- Lam, K. S., Salmon, S. E., Hersh, E. M., Hruby, V. J., Kazmierski, W. M., & Knapp, R. J. (1991). A new type of synthetic peptide library for identifying ligand-binding activity. *Nature*, *354*, 82–84. <https://doi.org/10.1038/354082a0>
- Lavoie, R., di Fazio, A., Blackburn, R., Goshe, M., Carbonell, R., & Menegatti, S. (2019). Targeted capture of Chinese hamster ovary host cell proteins: Peptide ligand discovery. *International Journal of Molecular Sciences*, *20*, 1729. <https://doi.org/10.3390/ijms20071729>
- Lavoie, R. A., Chu, W., Lavoie, J. H., Hetzler, Z., Williams, T. I., Carbonell, R., & Menegatti, S. (2021). Removal of host cell proteins from cell culture fluids by weak partitioning chromatography using peptide-based adsorbents. *Separation and Purification Technology*, *257*, 117890. <https://doi.org/10.1016/j.seppur.2020.117890>
- Lebl, M., Krchnák, V., Salmon, S. E., & Lam, K. S. (1994). Screening of completely random one-bead one-peptide libraries for activities in

- solution. *Methods*, 6, 381–387. <https://doi.org/10.1006/meth.1994.1038>
- Leikas, A. J., Hassinen, I., Hedman, A., Kivelä, A., Ylä-Herttua, S., & Hartikainen, J. E. K. (2022). Long-term safety and efficacy of intramyocardial adenovirus-mediated VEGF-DΔNΔC gene therapy eight-year follow-up of phase I KAT301 study. *Gene Therapy*, 29, 289–293. <https://doi.org/10.1038/s41434-021-00295-1>
- Levy, H. C., Bowman, V. D., Govindasamy, L., McKenna, R., Nash, K., Warrington, K., Chen, W., Muzyczka, N., Yan, X., Baker, T. S., & Agbandje-McKenna, M. (2009). Heparin binding induces conformational changes in adeno-associated virus serotype 2. *Journal of Structural Biology*, 165, 146–156. <https://doi.org/10.1016/j.jsb.2008.12.002>
- Li, C., & Samulski, R. J. (2020). Engineering adeno-associated virus vectors for gene therapy. *Nature Reviews Genetics*, 21, 255–272.
- Linden, R. M., Ward, P., Giraud, C., Winocour, E., & Berns, K. I. (1996). Site-specific integration by adeno-associated virus. *Proceedings of the National Academy of Sciences*, 93, 11288–11294.
- Lins-Austin, B., Patel, S., Mietzsch, M., Brooke, D., Bennett, A., Venkatakrisnan, B., Van Vliet, K., Smith, A. N., Long, J. R., McKenna, R., Potter, M., Byrne, B., Boye, S. L., Bothner, B., Heilbronn, R., & Agbandje-McKenna, M. (2020). Adeno-associated virus (AAV) capsid stability and liposome remodeling during endo/lysosomal pH trafficking. *Viruses*, 12, 668. <https://doi.org/10.3390/v12060668>
- Madhavi Sastry, G., Adzhigirey, M., Day, T., Annabhimoju, R., & Sherman, W. (2013). Protein and ligand preparation: Parameters, protocols, and influence on virtual screening enrichments. *Journal of Computer-Aided Molecular Design*, 27, 221–234. <https://doi.org/10.1007/s10822-013-9644-8>
- Magrin, E., Semeraro, M., Hebert, N., Joseph, L., Magnani, A., Chalumeau, A., Gabrion, A., Roudaut, C., Marouene, J., Lefrere, F., Diana, J. S., Denis, A., Neven, B., Funck-Brentano, I., Negre, O., Renolleau, S., Brousse, V., Kiger, L., Touzot, F., ... Cavazzana, M. (2022). Long-term outcomes of lentiviral gene therapy for the β-hemoglobinopathies: The HGB-205 trial. *Nature Medicine*, 28, 81–88.
- Mandel, R. J., & Burger, C. (2004). Clinical trials in neurological disorders using AAV vectors: Promises and challenges. *Current opinion in molecular therapeutics*, 6, 482–490.
- McIntosh, J., Lenting, P. J., Rosales, C., Lee, D., Rabbanian, S., Raj, D., Patel, N., Tuddenham, E. G. D., Christophe, O. D., McVey, J. H., Waddington, S., Nienhuis, A. W., Gray, J. T., Fagone, P., Mingozzi, F., Zhou, S. Z., High, K. A., Cancio, M., Ng, C. Y. C., ... Nathwani, A. C. (2013). Therapeutic levels of FVIII following a single peripheral vein administration of rAAV vector encoding a novel human factor VIII variant. *Blood, The Journal of the American Society of Hematology*, 121, 3335–3344.
- Merten, O. W., Gény-Fiamma, C., & Douar, A. M. (2005). Current issues in adeno-associated viral vector production. *Gene Therapy*, 12, S51–S61. <https://doi.org/10.1038/sj.gt.3302615>
- Mietzsch, M., Jose, A., Chipman, P., Bhattacharya, N., Daneshparvar, N., McKenna, R., & Agbandje-McKenna, M. (2021). Completion of the AAV structural Atlas: Serotype capsid structures reveals clade-specific features. *Viruses*, 13, 101.
- Mietzsch, M., Smith, J. K., Yu, J. C., Banala, V., Emmanuel, S. N., Jose, A., Chipman, P., Bhattacharya, N., McKenna, R., & Agbandje-McKenna, M. (2020). Characterization of AAV-specific affinity ligands: Consequences for vector purification and development strategies. *Molecular Therapy: Methods & Clinical Development*, 19, 362–373. <https://doi.org/10.1016/j.omtm.2020.10.001>
- Milone, M. C., & O'Doherty, U. (2018). Clinical use of lentiviral vectors. *Leukemia*, 32, 1529–1541.
- Moskalenko, M., Chen, L., van Roey, M., Donahue, B. A., Snyder, R. O., McArthur, J. G., & Patel, S. D. (2000). Epitope mapping of human anti-adeno-associated virus type 2 neutralizing antibodies: Implications for gene therapy and virus structure. *Journal of Virology*, 74, 1761–1766.
- Muhuri, M., Maeda, Y., Ma, H., Ram, S., Fitzgerald, K. A., Tai, P. W. L., & Gao, G. (2021). Overcoming innate immune barriers that impede AAV gene therapy vectors. *Journal of Clinical Investigation*, 131. <https://doi.org/10.1172/jci143780>
- Mukherjee, R. P., Yow, G.-Y., Sarakbi, S., Menegatti, S., Gurgel, P. V., Carbonell, R. G., & Bobay, B. G. (2023). Integrated in silico and experimental discovery of trimeric peptide ligands targeting butyrylcholinesterase. *Computational Biology and Chemistry*, 102, 107797.
- Nadeau, I., & Kamen, A. (2003). Production of adenovirus vector for gene therapy. *Biotechnology Advances*, 20, 475–489. [https://doi.org/10.1016/S0734-9750\(02\)00030-7](https://doi.org/10.1016/S0734-9750(02)00030-7)
- Nam, H.-J., Gurda, B. L., McKenna, R., Potter, M., Byrne, B., Salganik, M., Muzyczka, N., & Agbandje-McKenna, M. (2011). Structural studies of adeno-associated virus serotype 8 capsid transitions associated with endosomal trafficking. *Journal of Virology*, 85, 11791–11799. <https://doi.org/10.1128/JVI.05305-11>
- Nam, H.-J., Lane, M. D., Padron, E., Gurda, B., McKenna, R., Kohlbrenner, E., Aslanidi, G., Byrne, B., Muzyczka, N., Zolotukhin, S., & Agbandje-McKenna, M. (2007). Structure of adeno-associated virus serotype 8, a gene therapy vector. *Journal of Virology*, 81, 12260–12271.
- Naso, M. F., Tomkowicz, B., Perry, W. L., & Strohl, W. R. (2017). Adeno-associated virus (AAV) as a vector for gene therapy. *BioDrugs*, 31, 317–334.
- Okada, T., Nonaka-Sarukawa, M., Uchibori, R., Kinoshita, K., Hayashita-Kinoh, H., Nitahara-Kasahara, Y., Takeda, S., & Ozawa, K. (2009). Scalable purification of adeno-associated virus serotype 1 (AAV1) and AAV8 vectors, using dual ion-exchange adsorptive membranes. *Human Gene Therapy*, 20, 1013–1021. <https://doi.org/10.1089/hum.2009.006>
- Olsson, M. H. M., Søndergaard, C. R., Rostkowski, M., & Jensen, J. H. (2011). PROPKA3: Consistent treatment of internal and surface residues in empirical pKa predictions. *Journal of Chemical Theory and Computation*, 7, 525–537. <https://doi.org/10.1021/ct100578z>
- Parrinello, M., & Rahman, A. (1981). Polymorphic transitions in single crystals: A new molecular dynamics method. *Journal of Applied Physics*, 52, 7182–7190. <https://doi.org/10.1063/1.328693>
- Penzes, J. J., Chipman, P., Bhattacharya, N., Zeher, A., Huang, R., McKenna, R., & Agbandje-McKenna, M. (2021). Adeno-associated virus 9 structural rearrangements induced by endosomal trafficking pH and glycan attachment. *Journal of Virology*, 95, e0084321. <https://doi.org/10.1128/jvi.00843-21>
- Pérez, J. J., Pham, H. T., Chipman, P., Bhattacharya, N., McKenna, R., Agbandje-McKenna, M., & Tijssen, P. (2020). Molecular biology and structure of a novel penaeid shrimp densovirus elucidate convergent parvoviral host capsid evolution. *Proceedings of the National Academy of Sciences*, 117, 20211–20222. <https://doi.org/10.1073/pnas.2008191117>
- Petrich, J., Marchese, D., Jenkins, C., Storey, M., & Blind, J. (2020). Gene replacement therapy: A primer for the health-system pharmacist. *Journal of Pharmacy Practice*, 33, 846–855. <https://doi.org/10.1177/0897190019854962>
- Prodromou, R., Day, K. N., Saberi-Bosari, S., Schneible, J. D., Mabe, M. D., San Miguel, A., Daniele, M. A., Pozdin, V., & Menegatti, S. (2021). Engineering next generation cyclized peptide ligands for light-controlled capture and release of therapeutic proteins. *Advanced Functional Materials*, 31, 2101410. <https://doi.org/10.1002/adfm.202101410>
- Prodromou, R., Moore, B., Chu, W., Deal, H., San Miguel, A., Brown, A. C., Daniele, M. A., Aleksandrovich, V., & Menegatti, S. (2023). Molecular engineering of cyclic azobenzene-peptide hybrid ligands for the purification of human blood factor VIII via photo-affinity chromatography. *Advanced Functional Materials*, 33(14), 2213881.

- Qu, G., Bahr-Davidson, J., Prado, J., Tai, A., Cataniag, F., McDonnell, J., Zhou, J., Hauck, B., Luna, J., Sommer, J. M., Smith, P., Zhou, S., Colosi, P., High, K. A., Pierce, G. F., & Wright, J. F. (2007). Separation of adeno-associated virus type 2 empty particles from genome containing vectors by anion-exchange column chromatography. *Journal of Virological Methods*, *140*, 183–192. <https://doi.org/10.1016/j.jviromet.2006.11.019>.
- Rambhai, H. K., Ashby, F. J., Qing, K., & Srivastava, A. (2020). Role of essential metal ions in AAV vector-mediated transduction. *Molecular Therapy: Methods & Clinical Development*, *18*, 159–166.
- Reese, H. R., Xiao, X., Shanahan, C. C., Chu, W., Van Den Driessche, G. A., Fourches, D., Carbonell, R. G., Hall, C. K., & Menegatti, S. (2020). Novel peptide ligands for antibody purification provide superior clearance of host cell protein impurities. *Journal of Chromatography A*, *1625*, 461237. <https://doi.org/10.1016/j.chroma.2020.461237>
- Rostkowski, M., Olsson, M. H., S ndergaard, C. R., & Jensen, J. H. (2011). Graphical analysis of pH-dependent properties of proteins predicted using PROPKA. *BMC Structural Biology*, *11*, 6. <https://doi.org/10.1186/1472-6807-11-6>
- Rumachik, N. G., Malaker, S. A., Powell, N., Maynard, L. H., Adams, C. M., Leib, R. D., Cirolia, G., Thomas, D., Stamnes, S., Holt, K., Sinn, P., May, A. P., & Paulk, N. K. (2020). Methods matter: Standard production platforms for recombinant AAV produce chemically and functionally distinct vectors. *Molecular Therapy: Methods & Clinical Development*, *18*, 98–118. <https://doi.org/10.1016/j.omtm.2020.05.018>
- Saberi-Bosari, S., Omary, M., Lavoie, A., Prodromou, R., Day, K., Menegatti, S., & San-Miguel, A. (2019). Affordable microfluidic bead-sorting platform for automated selection of porous particles functionalized with bioactive compounds. *Scientific Reports*, *9*, 7210. <https://doi.org/10.1038/s41598-019-42869-5>
- Samaranch, L., Salegio, E. A., San Sebastian, W., Kells, A. P., Foust, K. D., Bringas, J. R., Lamarre, C., Forsayeth, J., Kaspar, B. K., & Bankiewicz, K. S. (2012). Adeno-associated virus serotype 9 transduction in the central nervous system of nonhuman primates. *Human Gene Therapy*, *23*, 382–389.
- Samulski, R. J., & Muzyczka, N. (2014). AAV-mediated gene therapy for research and therapeutic purposes. *Annual Review of Virology*, *1*, 427–451.
- Schmidt, M., Govindasamy, L., Afione, S., Kaludov, N., Agbandje-McKenna, M., & Chiorini, J. A. (2008). Molecular characterization of the heparin-dependent transduction domain on the capsid of a novel adeno-associated virus isolate, AAV (VR-942). *Journal of Virology*, *82*, 8911–8916.
- Sharma, A., Tiwari, V., & Sowdhagini, R. (2020). Computational search for potential COVID-19 drugs from FDA-approved drugs and small molecules of natural origin identifies several anti-virals and plant products. *Journal of Biosciences*, *45*, 100. <https://doi.org/10.1007/s12038-020-00069-8>
- Smith, R. H., Levy, J. R., & Kotin, R. M. (2009). A simplified baculovirus-AAV expression vector system coupled with one-step affinity purification yields high-titer rAAV stocks from insect cells. *Molecular Therapy*, *17*, 1888–1896. <https://doi.org/10.1038/mt.2009.128>
- Spiliotopoulos, D., Kastritis, P. L., Melquiond, A. S. J., Bonvin, A. M. J. J., Musco, G., Rocchia, W., & Spitaleri, A. (2016). dMM-PBSA: A new HADDOCK scoring function for protein-peptide docking. *Frontiers in Molecular Biosciences*, *3*. <https://doi.org/10.3389/fmolb.2016.00046>.
- Sripada, S. A., Chu, W., Williams, T. I., Teten, M. A., Mosley, B. J., Carbonell, R. G., Lenhoff, A. M., Cramer, S. M., Bill, J., Yigzaw, Y., Roush, D. J., & Menegatti, S. (2022). Towards continuous mAb purification: Clearance of host cell proteins from CHO cell culture harvests via “flow-through affinity chromatography” using peptide-based adsorbents. *Biotechnology and Bioengineering*, *119*(7), 1873–1889. <https://doi.org/10.1002/bit.28096>
- Stagg, S. M., Yoshioka, C., Davulcu, O., & Chapman, M. S. (2022). Cryo-electron microscopy of adeno-associated virus. *Chemical Reviews*, *122*, 14018–14054. <https://doi.org/10.1021/acs.chemrev.1c00936>
- Summerford, C., & Samulski, R. J. (1998). Membrane-associated heparan sulfate proteoglycan is a receptor for adeno-associated virus type 2 virions. *Journal of Virology*, *72*, 1438–1445.
- Thermo Scientific™. POROS™ CaptureSelect™ AAV Resins: AAV8, AAV9, AAVX. https://www.thermofisher.com/document-connect/document-connect.html?url=https://assets.thermofisher.com/TFS-Assets%2FLSG%2Fmanuals%2F100038399_POROS_CapSel_AAV8_AAV9_Resins_UG.pdf
- Thermo Scientific™. POROS™ CaptureSelect™ AAV8 Affinity Resin. <https://www.thermofisher.com/order/catalog/product/A30790>
- Thermo Scientific™. POROS™ CaptureSelect™ AAV9 Affinity Resin. <https://www.thermofisher.com/order/catalog/product/A27356?SID=srch-srp-A27356>
- Thermo Scientific™. POROS™ CaptureSelect™ AAVX Affinity Resin. https://www.thermofisher.com/order/catalog/product/A36741?ef_id=Cj0KCCQjwhqAVBhCxARIsAHK1tiMtK3Dgq-lhgCj3YQG6mG0tISlBqpecU8BUR-7kEe3dSdPTXQBDg0laAhQREALw_wcB:G:s&s_kwcid=AL!3652!3!595826604655!!!gclid=Cj0KCCQjwhqAVBhCxARIsAHK1tiMtK3Dgq-lhgCj3YQG6mG0tISlBqpecU8BUR-7kEe3dSdPTXQBDg0laAhQREALw_wcB
- Tu, M., Liu, F., Chen, S., Wang, M., & Cheng, A. (2015). Role of capsid proteins in parvovirus infection. *Virology Journal*, *12*, 114. <https://doi.org/10.1186/s12985-015-0344-y>
- Vasileva, A., & Jessberger, R. (2005). Precise hit: Adeno-associated virus in gene targeting. *Nature Reviews Microbiology*, *3*, 837–847.
- Wang, D., Tai, P. W. L., & Gao, G. (2019). Adeno-associated virus vector as a platform for gene therapy delivery. *Nature Reviews Drug Discovery*, *18*, 358–378.
- Wang, R. Z., Lin, D.-Q., Chu, W.-N., Zhang, Q.-L., & Yao, S.-J. (2016). New tetrapeptide ligands designed for antibody purification with biomimetic chromatography: Molecular simulation and experimental validation. *Biochemical Engineering Journal*, *114*, 191–201. <https://doi.org/10.1016/j.bej.2016.06.030>
- Wold, W. S. M., & Toth, K. (2013). Adenovirus vectors for gene therapy, vaccination and cancer gene therapy. *Current Gene Therapy*, *13*, 421–433.
- Wu, Z., Asokan, A., Grieger, J. C., Govindasamy, L., Agbandje-McKenna, M., & Samulski, R. J. (2006). Single amino acid changes can influence titer, heparin binding, and tissue tropism in different adeno-associated virus serotypes. *Journal of Virology*, *80*, 11393–11397. <https://doi.org/10.1128/jvi.01288-06>
- Xiao, X., Kilgore, R., Sarma, S., Chu, W., Menegatti, S., & Hall, C. K. (2022). De novo discovery of peptide-based affinity ligands for the Fab fragment of human immunoglobulin G. *Journal of Chromatography A*, *1669*, 462941. <https://doi.org/10.1016/j.chroma.2022.462941>
- Xie, Q., Bu, W., Bhatia, S., Hare, J., Somasundaram, T., Azzi, A., & Chapman, M. S. (2002). The atomic structure of adeno-associated virus (AAV-2), a vector for human gene therapy. *Proceedings of the National Academy of Sciences*, *99*, 10405–10410.
- Zincarelli, C., Soltys, S., Rengo, G., & Rabinowitz, J. E. (2008). Analysis of AAV serotypes 1–9 mediated gene expression and tropism in mice after systemic injection. *Molecular Therapy*, *16*, 1073–1080.
- Zolotukhin, S., Potter, M., Zolotukhin, I., Sakai, Y., Loiler, S., Fraities, Jr., T. J., Chiodo, V. A., Phillipsberg, T., Muzyczka, N., Hauswirth, W. W., Flotte, T. R., Byrne, B. J., & Snyder, R. O. (2002). Production and purification of serotype 1, 2, and 5 recombinant adeno-associated viral vectors. *Methods*, *28*, 158–167.

van Zundert, G. C. P., Rodrigues, J. P. G. L. M., Trellet, M., Schmitz, C., Kastiris, P. L., Karaca, E., Melquiond, A. S. J., van Dijk, M., de Vries, S. J., and Bonvin, A. M. J. J. (2016). The HADDOCK2.2 web server: User-friendly integrative modeling of biomolecular complexes. *Journal of Molecular Biology* 428, 720–725. <https://doi.org/10.1016/j.jmb.2015.09.014>.

SUPPORTING INFORMATION

Additional supporting information can be found online in the Supporting Information section at the end of this article.

How to cite this article: Chu, W., Shastry, S., Barbieri, E., Prodromou, R., Greback-Clarke, P., Smith, W., Moore, B., Kilgore, R., Cummings, C., Pancorbo, J., Gilleskie, G., Daniele, M. A., & Menegatti, S. (2023). Peptide ligands for the affinity purification of adeno-associated viruses from HEK 293 cell lysates. *Biotechnology and Bioengineering*, 120, 2283–2300. <https://doi.org/10.1002/bit.28495>